MULTIPLE EXCITON GENERATION IN GRAPHENE NANOSTRUCTURES

A Thesis Submitted to
the Graduate School of Engineering and Sciences of
İzmir Institute of Technology
in Partial Fulfillment of the Requirements for the Degree of

MASTER OF SCIENCE

in Physics

by
Jülide YILDIRIM

November 2014
İZMİR

We approve the thesis of **Jülide YILDIRIM**

Examining Committee Members:

Assoc. Prof. Dr. Özgür ÇAKIR
Department of Physics, Izmir Institute of Technology

Prof. Dr. R. Tuğrul SENGER
Department of Physics, Izmir Institute of Technology

Assoc. Prof. Dr. Hâldun SEVİNÇLİ
Department of Materials Science and Engineering, Izmir Institute of Technology

7 November 2014

Assoc.Prof. Dr. Özgür ÇAKIR
Supervisor, Department of Physics
Izmir Institute of Technology

Prof. Dr. Nejat BULUT
Head of the Department of Physics

Prof. Dr. R. Tuğrul SENGER
Dean of the Graduate School of
Engineering and Sciences

ACKNOWLEDGMENTS

I would like to thank my supervisor Assoc. Prof. Dr. Özgür Çakır for guidance, support and patience throught this thesis period. He has always been willing to listen to any problem and to provide helpful suggestions.

I would like to thank to the other members of my defence committee, Prof. Dr. R. Tuğrul Senger and Assoc. Prof. Dr. Haldun Sevinçli for helpful comments and giving suggestions.

I thank all my friends at İzmir Institute of Technology for their warm friendship and enjoyable times we spent. I also want to thank to Erdi Kuşdemir, Zafer Kandemir, Funda Mıdık, Gözde Özbal, Beyhan Puliçe, Hemza Azri for their friendship and support.

Finally, a big thanks to my dear family for their endless support, encouragement, motivation and love during all my life.

ABSTRACT

MULTIPLE EXCITON GENERATION IN GRAPHENE NANOSTRUCTURES

This thesis comprises a theoretical study on the role of the inverse-Auger process in graphene nanostructures. Inverse-Auger effect (IAE) is the formation of a multitude of low energy excitons from a single exciton of higher energy. Its mechanism is the conversion of the kinetic energy of the high energy carriers to new excitons via Coulomb interaction. Bulk graphene has zero band gap energy and has two Dirac points which is linearly dependent crystal momentum. Due to quantum confinement, graphene nanoribbons and graphene flakes or the structures having periodically holes develop a band gap. The emergence of a band gap makes these structures eligible for solar cell applications. In bulk structures, due to translational symmetry momentum is conserved which leads to a decreased IAE. However, in nanostructures, in addition to the relaxation of momentum conservation condition, the Coulomb interaction between the carriers increases which leads to an enhanced IAE. In this thesis, a theoretical analysis of inverse-Auger effect is carried out for graphene and armchair graphene nanoribbons. Tight binding method is employed to obtain the electronic structure and to calculate the Coulomb matrix elements for the inverse-Auger effect in this structures. According to our calculations, inverse-Auger effect in the bulk graphene provides the formation of new excitons at a rate which is approximately linearly proportional to the energy of an electron at the conduction band.

ÖZET

GRAFEN NANO YAPILARDA ÇOKLU EKSİTON OLUŞUMU

Bu tez grafen nano yapılarda ters-Auger prosesinin teorik analizini kapsamaktadır. Ters-Auger etkisi yüksek enerjili bir egzitondan enerji korunumunun izin verdiği ölçüde daha düşük enerjili egzitonların oluşmasıdır. Mekanizması ise Coulomb etkileşimi vasıtasıyla yüksek enerjili yüklerin kinetik enerjilerinin yeni egzitonlara çevrimidir. Yığın grafen sıfır bant aralığına sahiptir, ve kristal momentuma lineer olarak bağımlı iki adet Dirac noktasına sahiptir. Grafen nano-pullarda, grafen şeritlerde periyodik olarak deliklere sahip grafen yapılarda kuantum boyut etkisi nedeniyle bir bant aralığı oluşabilmektedir. Bir band aralığının ortaya çıkması güneş pili uygulamaları için, bu yapıları uygun hale getirir. Yığın yapılar yer değiştirme altında simetriye sahip olduğu için momentum korunmakta, bu da ters-Auger hızını azaltmaktadır. Fakat nano yapılarda momentum korunumu şartının gevşemesi yanında, Coulomb etkileşiminin etkisi artmakta bu da ters-Auger hızını artırmaktadır. Bu tezde ters-Auger etkisi grafen nano yapılarda teorik olarak incelenmiştir. Bu yapıların elektronik yapılarını elde etmek ve Coulomb matris öğelerini hesaplamak için sıkı bağlanma yöntemi kullanılmıştır. Yaptığımız hesaplara göre, grafen yığınlarında ters-Auger etkisi, iletim bandındaki bir elektronun enerjisiyle yaklaşık olarak doğru orantılı bir şekilde yeni eksitonların oluşumunu sağlamaktadır.

TABLE OF CONTENTS

LIST OF FIGURES

Figure **Page**

CHAPTER 1

INTRODUCTION

The Auger effect was discovered in 1925 by Pierre Auger in gases and expressed as follows. In an inner shell, when an atom is ionized, one of the electrons at the higher orbit drops into vacancy and the other receives energy which is used to remove it from the atom. In 1958, the significance of the Auger effect was recognized in the solid state. It was proved to be important for semiconductors. It can be crucial for devices whose performance is governed by lifetimes. Radiative transition is accompanied by an emission of photon whereas the Auger effect is a non-radiative process. The Auger recombination rate behaves as n^2p or p^2n where n is the electron density and p is the hole density while the radiative rate behaves as np. The reverse process of the Auger recombination called impact ionization employ this type of process. In the impact ionization process, one extra particle is generated as follows [2]

$$\begin{aligned} e &\rightarrow 2e + h \\ h &\rightarrow 2h + e \end{aligned} \tag{1.1}$$

Inverse-Auger effect also known as the carrier multiplication is a non-radiative mechanism which leads to formation of a multitude of low energy excitons from a single exciton of higher energy. The driving mechanism is the Coulomb interaction, in which electrons or holes lose their kinetic energy giving rise to a new electron-hole pair. In bulk structures, due to translational symmetry momentum is conserved, which leads to a decreased inverse-Auger effect. However, in nanostructures there are a couple of factors which lead to an enhanced inverse-Auger effect. Due to quantum confinement the energy is quantized and momentum is no longer a good quantum number. In addition in a nanostructure Coulomb interaction between the carriers is also enhanced. Another factor is the suppressed phonon induced cooling, where phonon energies are not sufficient for inducing electronic transitions due to discrete energy levels. Therefore, we expect an enhanced inverse Auger effect in nanostructures. Carrier multiplication effect has the

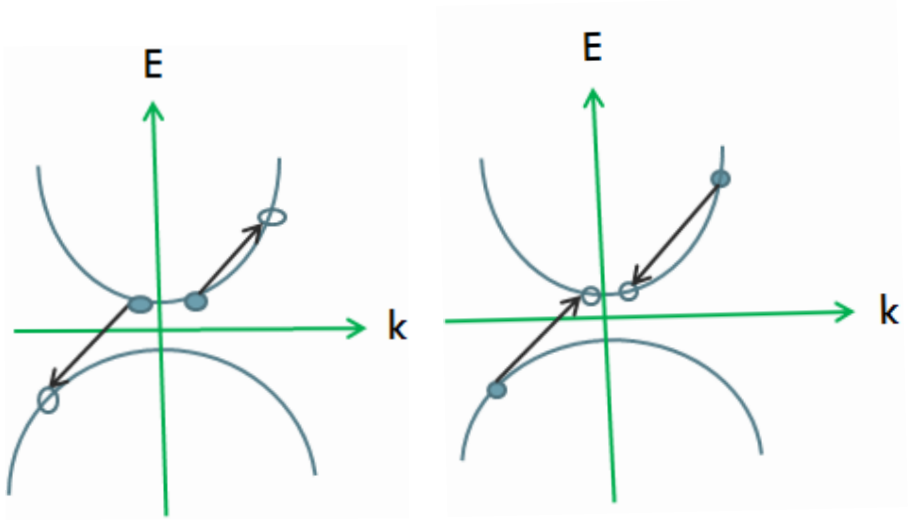

Figure 1.1. Left,schematic of Auger process. Right, schematic of inverse-Auger process.

potential to improve the performance of photovoltaic devices and the device's transport properties. It has been observed and studied for quantum dots [3, 4] and carbon nanotubes [5, 6]. Starting around 2005, PbSe and PbS quantum dots having the low-band gap and high Bohr radius were reported to exhibit carrier multiplication, i.e. an incident single photon producing multiple excitons. Afterwards, the approach in this experiment is used for the explanation of multi exciton generation by Efros's group. The solution of electronical and optical properties of PbSe and PbS quantum dots by effective mass method with the four band Hamiltonian was introduced by Kang and Wise. In the time-dependent photo-luminescence measurements the quantum yields based upon the principle of the faster multi exciton generation were determined [1, 4] (FIG. 1.2)

The high quantum yields in the results that are obtained from the first experiments were found at the lower values than the subsequent experiments [7]. There is evidence that surface charge states of nanocrystals lead to misleading results at the first experiments. The findings related to the generation of multi exciton have been observed in carbon nanotubes fotodiodes [5]. In this experiment when the photon energies correspond to the band gap's multitudes, the current jumps were observed. In solar cell applications carrier multiplication enables production of a multitude of electron-hole pairs per single photon, which will eventually increase the efficiency of light energy to electric energy conversion. On the other hand, carriers confined in nanostructures offer electrical/optical control over their quantum states, which makes them candidates for quantum information processing.

The key objective of this work is to contribute to an understanding of the carrier

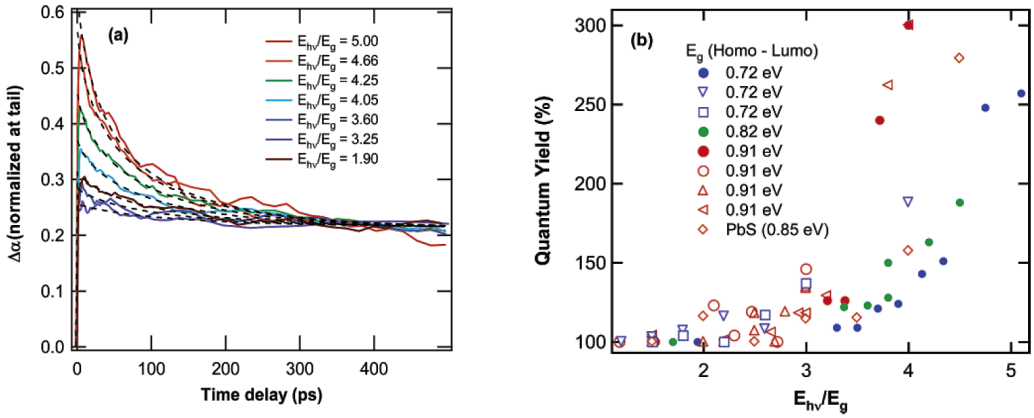

Figure 1.2. Exciton population decay dynamics obtained by probing intraband transitions and quantum yield for exciton formation [1].

multiplication dynamics in graphene nanostructures by means of a theoretical approach. Graphene consists of a single layer hexagonal lattice of carbon atoms. In contrast to conventional semiconductors having a band gap and a parabolic band structure, graphene shows the unusual linear, gapless band structure leading to unique electronic and optical properties. Auger processes in graphene were addressed first by F. Rana [8]. An increasing number of experimental indications for carrier multiplication in graphene have been found recently [9, 10, 11]. Graphene nanoribbons have unique electronic and optical properties. They have quasi one dimensional (1D) structures and are finite width graphene strips. Their band structure are determined by the edge shape of graphene nanoribbons. Zigzag nanoribbons give metalic properties while armchair structures can produce both semiconductor and metalic structures. In optoelectronic devices, armchair graphene nanoribbons having a tunable band gap are used as an alternative structures. The energy gap of armchair nanoribbons can be detuned by changing width or by inducing an electric field on these structures. In recent studies , the role of Auger scattering consisting of Auger recombination and impact ionization in graphene [8, 12, 13] , graphene nanoribbons and finite graphene nanostructures is performed [14, 15].

In this thesis, we investigate the inverse-Auger rate for bulk graphene and armchair nanoribbon by using the tight binding method. Firstly, in chapter 2, we represent the electronic structure of the bulk graphene obtained from tight binding method theoretically. Then, we calculate the inverse-Auger rate. In chapter 3, the electronic structure and inverse-Auger rate of the armchair graphene nanoribbon is studied by using tight binding method.

CHAPTER 2

INVERSE AUGER EFFECT IN GRAPHENE

2.1. The Tight binding Model of Graphene

In the last decade, graphene having unusual physical properties has emerged as a new material for high speed electronics [16, 17, 18, 19]. Graphene has two dimensional (2D) nature with the energy dispersion $E = \pm\hbar v_F k$ where k is the electron momentum $k = \sqrt{k_x^2 + k_y^2}$ and $v_F \sim 10^8 cm/s$ is Fermi velocity same for all carriers [20, 21, 22]. Graphene is a sp^2 carbon allotrope system with particular electrical, mechanical and optical characteristics. Structurally graphene has two sites per unit cell (two sublattices A and B) and is made of carbon atoms arranged in honeycomb hexagonal lattice where each carbon atom is covalently bonded with three neighboring atoms at a distance $a_{C-C} \simeq 1.42\mathring{A}$. The sp^2 hybridization in carbon atoms allows the presence of σ orbitals. The σ orbitals obtained from p_x, p_y and s orbitals lead to a hexagonal planar structure and are responsible for covalent bonding between neighboring C atoms that forms the basis of the extremely high mechanical stability of this material. On the other hand, the energies of the σ bonds are far away from the Fermi level and do not contribute in the electrical and optical characteristics of graphene. The remaining π orbitals obtained from p_z electron are perpendicular to the lattice surface and are responsible for the peculiarity of its low-energy electronic properties. Since only the p_z orbital is close to Fermi level the tight binding method consider the p_z orbitals.

The vectors identifying the the position of the unit cell are

$$\vec{R}_j = n\vec{a}_1 + m\vec{a}_2 \tag{2.1}$$

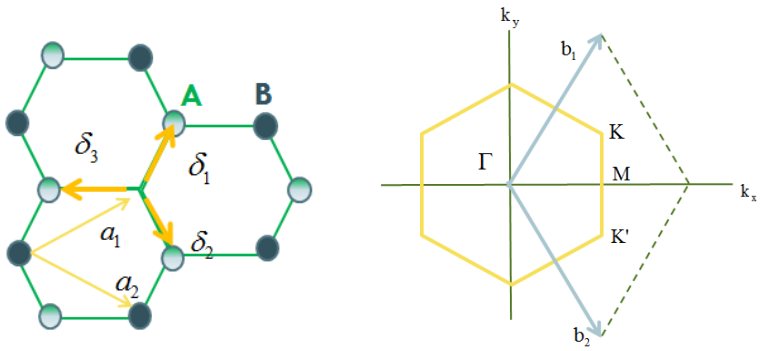

Figure 2.1. Left, schematic of graphene unit cell with basic lattice vectors. Right, the Brillouin zone of graphene.

where $j = (m, n)$. $\vec{a}_1$ and $\vec{a}_2$ vectors are defined as

$$\begin{aligned} \vec{a}_1 &= \frac{a\sqrt{3}}{2}x + \frac{3a}{2}y \\ \vec{a}_2 &= -\frac{a\sqrt{3}}{2}x + \frac{3a}{2}y \end{aligned} \tag{2.2}$$

where a is the distance between two nearest neighbors. If the positions of the A atoms can be choosen as the position of the unit cells for simplicity

$$\vec{R}_j^A = \vec{R}_j \tag{2.3}$$

then the B atoms are located at

$$\vec{R}_j^B = \vec{R}_j + \vec{\delta}_3 \tag{2.4}$$

The three vectors connecting an atom A with its three nearest neighbors can be written as:

$$\vec{\delta_1} = \frac{a\sqrt{3}}{2}x + \frac{a}{2}y$$
$$\vec{\delta_2} = -\frac{a\sqrt{3}}{2}x + \frac{a}{2}y$$
$$\vec{\delta_3} = -ay \tag{2.5}$$

The Hamiltonian for hoppings between the nearest neighbor sites can be written as

$$H = -t\sum_{<i,j>} a_i^\dagger b_j - t\sum_{<i,j>} b_i^\dagger a_j \tag{2.6}$$

where $< i, j >$ is nearest neigbors. Since there are three types of nearest neighbor bonds we write the Hamiltonian as

$$H = -t\sum_i a^\dagger_{\vec{R}_i} b_{R_i+\vec{\delta}_1} - t\sum_i a^\dagger_{\vec{R}_i} b_{R_i+\vec{\delta}_2} - t\sum_i a^\dagger_{\vec{R}_i} b_{R_i+\vec{\delta}_3} + h.c. \tag{2.7}$$

Here the sum $\sum_i$ sums over all unit cells.Using the Fourier transformation of a_i and b_i we get

$$a_k = \frac{1}{\sqrt{N}}\sum_i a_i e^{i\vec{k}.\vec{R}}$$
$$a_i = \frac{1}{\sqrt{N}}\sum_k a_k e^{-i\vec{k}.\vec{R}}$$
$$b_k = \frac{1}{\sqrt{N}}\sum_i b_i e^{i\vec{k}.\vec{R}}$$
$$b_i = \frac{1}{\sqrt{N}}\sum_k b_k e^{-i\vec{k}.\vec{R}} \tag{2.8}$$

We need to change $a^\dagger_{\vec{R}_i} b_{\vec{R}_i+\vec{\delta}_1}$ into $a_k^\dagger b_k$ and change sum over all unit cells into sum over all momentum points in order to calculate the terms in the Hamiltonian. Thus, we can

calculate the first term in the Hamiltonian

$$\begin{aligned}
-t\sum_i a^\dagger_{\vec{R}_i} b_{\vec{R}_i+\vec{\delta}_1} &= -\frac{t}{N}\sum_i\sum_k\sum_{k'} a^\dagger_k e^{i\vec{k}.\vec{R}_i} b_{k'} e^{-i\vec{k}'.(\vec{R}_i+\vec{\delta}_1)} \\
&= -t\sum_k\sum_{k'} a^\dagger_k b_{k'} e^{-i\vec{k}'.\vec{\delta}_1}\frac{1}{N}\sum_i e^{i(\vec{k}-\vec{k}').\vec{R}_i} \\
&= -t\sum_k\sum_{k'} a^\dagger_k b_{k'} e^{-i\vec{k}'.\vec{\delta}_1}\delta_{k,k'} \\
&= -t\sum_k a^\dagger_k b_k e^{-i\vec{k}'.\vec{\delta}_1}
\end{aligned} \tag{2.9}$$

Similarly, the other terms in the Hamiltonian can be calculated

$$\begin{aligned}
H &= -t\sum_i a^\dagger_{\vec{R}_i} b_{R_i+\vec{\delta}_1} - t\sum_i a^\dagger_{\vec{R}_i} b_{R_i+\vec{\delta}_2} - t\sum_i a^\dagger_{\vec{R}_i} b_{R_i+\vec{\delta}_3} + h.c. \\
&= -t\sum_k a^\dagger_k b_k\left(e^{-i\vec{k}.\vec{\delta}_1} + e^{-i\vec{k}.\vec{\delta}_2} + e^{-i\vec{k}.\vec{\delta}_3}\right) - t\sum_k b^\dagger_k a b_k\left(e^{i\vec{k}.\vec{\delta}_1} + e^{i\vec{k}.\vec{\delta}_2} + e^{i\vec{k}.\vec{\delta}_3}\right) \\
&= \sum_k (a^\dagger_k b^\dagger_k)\begin{pmatrix} 0 & f(\vec{k}) \\ f^*(\vec{k}) & 0 \end{pmatrix}\begin{pmatrix} a_k \\ b_k \end{pmatrix}
\end{aligned} \tag{2.10}$$

where $f(\vec{k})$ is defined as

$$f(\vec{k}) = -t(e^{-i\vec{k}\vec{\delta}_1} + e^{-i\vec{k}\vec{\delta}_2} + e^{-i\vec{k}\vec{\delta}_3}) \tag{2.11}$$

The diagonalization of this matrix gives the band dispersion relation

$$\epsilon(\vec{k}) = \pm|f(\vec{k})| = \pm t\sqrt{3 + 2\cos(\sqrt{3}k_x a) + 4\cos(\sqrt{3}k_x a/2)\cos(3k_y a/2)} \tag{2.12}$$

where '+' is for the upper band and '-' is for the lower band.

2.2. Auger and Inverse Auger Process in Graphene

The linear and gapless bandstructure of graphene allows for efficient Auger-type scattering processes.The Auger recombination describes the annihilation of an electron-hole pair, while the processes creating an electron-hole pair are denoted inverse-Auger. Inverse-Auger provides the possibility of multiple charge carrier generation by absorbing a single photon. Therefore, the inverse-Auger plays an important role for the design of photodetectors or photovoltaic devices. Recently studies on carrier multiplication has been reported in semiconductor quantum dots, carbon nanotubes, nanoribbons and finite graphene nanostructures. In quantum dots and carbon nanotubes, the carrier multiplication has been approved experimentally. The scattering rates for Auger recombination and generation in graphene addressed first by F. Rana [8] have been derived for inverted electron-hole populations for which the scattering times were found longer than 1ps for concentrations less than $10^{12}/cm^2$.

2.2.1. Inverse Auger Rate Calculation in Graphene

In this section, a detailed analysis of inverse-Auger process in graphene is presented. We calculate the inverse-Auger process for intraband scattering.

The Bloch functions for the conduction $(s = +1)$ and valence $(s = -1)$ band electrons in graphene can be written as

$$\psi_{s,\mathbf{k}}(r) = \frac{e^{i\mathbf{k}.\mathbf{r}}}{\sqrt{N}} u_{s,\mathbf{k}}(r) \tag{2.13}$$

The single particle tight binding wave functions have the form [23]

$$u_k(r) = \frac{1}{\sqrt{2}} \sum_R \left[\chi_A(r - R_A) \mp e^{i\varphi_k} \chi_B(r - R_B)\right] e^{ik.(R-r)} \tag{2.14}$$

$$\phi_{s,k}(r) = \frac{1}{\sqrt{N}} \sum C^{\gamma}_{s,k} e^{ik.R} \chi^{\gamma}(r - R) \tag{2.15}$$

with N the number of graphene unit cells. Here, $\chi^{\gamma}(r - R)$ are the $2p_z$ atomic orbitals located at the lattice positions R, where $\gamma = A, B$ labels the two sublattices and 'k' is the electronic wave number. Thus, we can write the wave function for conduction and

valance band

$$\phi_k^c(r) = \frac{1}{\sqrt{N}} \sum \frac{1}{\sqrt{2}} \left(\chi^A(r-R) + e^{i\varphi_k}\chi^B(r-R)\right) e^{i\vec{k}.\vec{R}} \tag{2.16}$$

$$\phi_k^v(r) = \frac{1}{\sqrt{N}} \sum \frac{1}{\sqrt{2}} \left(\chi^A(r-R) - e^{i\varphi_k}\chi^B(r-R)\right) e^{i\vec{k}.\vec{R}} \tag{2.17}$$

$$s_1' = s_1 = c, s_2' = c, s_2 = v$$

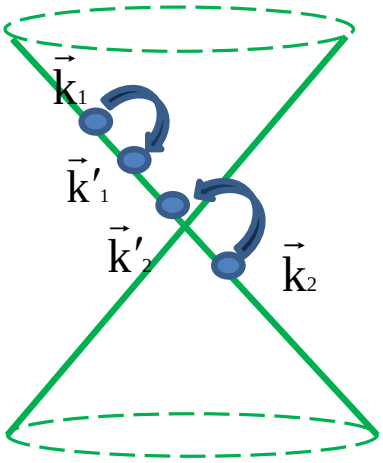

Figure 2.2. Inverse-Auger process for intravalley scattering in graphene.

The electron- hole generation rate Γ can be written as

$$\Gamma = \left(\frac{2\pi}{\hbar}\right) \sum_{k_2 k_1' k_2'} |M|^2 f_{k_2 v}(1 - f_{k_{1'c}})(1 - f_{k_{2'c}})$$
$$\times \delta(\hbar\nu|k_1 + Q| + \hbar\nu|k_2 - Q| - \hbar\nu|k_1| + \hbar\nu|k_2|) \tag{2.18}$$

where M is the coulomb matrix elements [24, 8, 25] including the direct and exchange interaction between electrons.

$$\Gamma = \left(\frac{2\pi}{\hbar}\right) \sum_{k_2 Q} |\left\langle k_1' c\sigma_1'; k_2' c\sigma_2' | V(r_1 - r_2) | k_1 c\sigma_1; k_2 v\sigma_2 \right\rangle|^2$$
$$\times f_{k_2 v\sigma_2}(1 - f_{k_{1'c}\sigma_1'})(1 - f_{k_{2'c}\sigma_2'})$$
$$\times \delta(\hbar\nu|k_1 + Q| + \hbar\nu|k_2 - Q| - \hbar\nu|k_1| + \hbar\nu|k_2|) \tag{2.19}$$

If we consider the summation over all spin states then the transition probability can be rewritten as

$$\Gamma = \frac{2\pi}{\hbar}\sum\frac{1}{4}|\left\langle\phi_{k_1'}(1)\phi_{k_2'}(2)+\phi_{k_1'}(2)\phi_{k_2'}(1)|V|\phi_{k_1}(1)\phi_{k_2}(2)+\phi_{k_1}(2)\phi_{k_2}(1)\right\rangle|^2$$
$$+\frac{2\pi}{\hbar}3\sum\frac{1}{4}|\left\langle\phi_{k_1'}(1)\phi_{k_2'}(2)-\phi_{k_1'}(2)\phi_{k_2'}(1)|V|\phi_{k_1}(1)\phi_{k_2}(2)-\phi_{k_1}(2)\phi_{k_1}(2)\phi_{k_2}(1)\right\rangle|^2$$
$$\times f_{k_2v}(1-f_{k_{1'_c}})(1-f_{k_{2'_c}})\delta(\hbar\nu|k_1+Q|+\hbar\nu|k_2-Q|-\hbar\nu|k_1|+\hbar\nu|k_2|) \quad (2.20)$$

First term describes the spin singlet, and second term describes the spin triplet condition. The arbitrary condition of spins indicates that spins exist 25% spin singlet and 75% spin triplet. Therefore we can rewrite the rate equation as

$$\Gamma = \frac{2\pi}{\hbar}\sum\frac{1}{4}\left(|2\left\langle 12|V|12\right\rangle+2\left\langle 12|V|21\right\rangle|^2+3|2\left\langle 12|V|12\right\rangle-\left\langle 12|V|21\right\rangle|^2\right)$$
$$\times f_{k_2v}(1-f_{k_{1'_c}})(1-f_{k_{2'_c}})\delta(\hbar\nu|k_1+Q|+\hbar\nu|k_2-Q|-\hbar\nu|k_1|+\hbar\nu|k_2|+) \quad (2.21)$$

where

$$M_d = \langle 12|V|12\rangle \quad (2.22)$$

$$M_e = \langle 12|V|21\rangle \quad (2.23)$$

M_d is the direct term and M_e is the exchange term of the matrix element and it is assumed that the scattering $k_1 \to k_1', k_2 \to k_2'$ is distinguishable from the exchange scattering $k_1 \to k_2', k_2 \to k_1'$. Squaring and summing over all spin states in the equations (2.19 and 2.20)

$$|M|^2 = \left(4(M_d^2+M_e^2)-4M_dM_e\right)$$
$$= 2|M_d-M_e|^2+2|M_d|^2+2|M_e|^2 \quad (2.24)$$

$$\Gamma = \left(\frac{2\pi}{\hbar}\right)\sum_{k_2k_1'k_2'}\left(4(M_d^2+M_e^2)-4M_dM_e\right)f_{k_2v}(1-f_{k_{1'_c}})(1-f_{k_{2'_c}})$$
$$\times\delta(\hbar\nu|k_1+Q|+\hbar\nu|k_2-Q|-\hbar\nu|k_1|+\hbar\nu|k_2|) \quad (2.25)$$

By inserting the tight binding wave function we can evaluate the direct term

$$M_d = \int d^2r_1 d^2r_2 \phi^*_{ck'_1}(1)\phi^*_{ck'_2}(2)V(r_1 - r_2)\phi_{vk_2}(2)\phi_{vk_1}(1) \tag{2.26}$$

where

$$\phi_{sk}(r) = \frac{1}{\sqrt{N}} \sum C^{\gamma}_{sk} e^{ik.R} \chi^{\gamma}(r - R) \tag{2.27}$$

C^{γ}_{sk} is the tight binding coefficient function and $\chi^{\gamma}(r-R)$ is the orbital functions centered at the position of the carbon atoms R.

$$\begin{aligned} M_d = \frac{1}{N^2} \int dr_1 dr_2 \sum_{R_1 R_2} C^{\gamma *}_{s'_1 k'_1} C^{\gamma}_{s_1 k_1} |\chi^{\gamma}(r_1 - R)|^2 e^{-i(k'_1 - k_1).R_1} \\ V(r_1 - r_2) C^{\gamma'^*}_{s'_2 k'_2} C^{\gamma'}_{s_2 k_2} |\chi^{\gamma'}(r_2 - R_2)|^2 e^{-i(k'_2 - k_2).R'} \end{aligned} \tag{2.28}$$

After introducing the relative coordinate and center of mass frame as follows

$$\begin{aligned} R &= \frac{R_1 + R_2}{2} \\ r &= R_1 - R_2 \\ R_1 &= R + \frac{r}{2} \\ R_2 &= R - \frac{r}{2} \end{aligned} \tag{2.29}$$

the direct matrix element reads

$$M_d = \frac{1}{N^2} \sum_{R_1 R_2} C^{\gamma *}_{s'_1 k'_1} C^{\gamma}_{s_1 k_1} e^{-i(k'_1 - k_1).(\vec{R} + \frac{\vec{r}}{2})} V(\vec{r}) C^{\gamma'^*}_{s'_2 k'_2} C^{\gamma'}_{s_2 k_2} e^{-i(k'_2 - k_2).(\vec{R} - \frac{\vec{r}}{2})} \tag{2.30}$$

$$\begin{aligned} M_d = \frac{1}{N^2} \sum_{R_1 R_2} C^{\gamma *}_{s'_1 k'_1} C^{\gamma}_{s_1 k_1} C^{\gamma'^*}_{s'_2 k'_2} C^{\gamma'}_{s_2 k_2} e^{-i(k'_1 + k'_2 - k_1 - k_2).\vec{R}} \\ \times e^{-i(k'_1 - k_1 - (k'_2 - k_2)).\frac{\vec{r}}{2}} V(\vec{r}) \end{aligned} \tag{2.31}$$

The conservation of momentum follows from Kronecker deltas which are acquired by performing the sum over the lattice vectors

$$\sum_{\vec{R}} e^{-i\sum k_i.R} = N\delta_{\sum k_i=0} \tag{2.32}$$

Fourier transform of 2D Coulomb potential is

$$\begin{aligned}\sum_{\vec{r}} e^{-iQ.\vec{r}}V(\vec{r}) &= \int \frac{d^2\vec{r}}{\Omega} e^{-iQ.\vec{r}}V(\vec{r}) \\ &= \frac{4\pi^2 e^4}{K^2 + (k_1' - k_1)^2}\end{aligned} \tag{2.33}$$

where K is the screening length

$$\begin{aligned}M_d = \sum cos\left(\frac{\varphi_{k_1'} - \varphi_{k_1}}{2}\right) sin\left(\frac{\varphi_{k_2'} - \varphi_{k_2}}{2}\right) \frac{1}{N}\delta_{(k_1'+k_2'-k_1-k_2=0)} \\ \times \frac{4\pi^2 e^4}{K^2 + (k_1' - k_1)^2}\end{aligned} \tag{2.34}$$

We can do same calculation for the exchange term

$$M_e = \int d^2r_1 d^2r_2 \phi^*_{s_1'k_1'}(1)\phi^*_{s_2'k_2'}(2)V(r_1 - r_2)\phi^*_{s_1k_1}(1)\phi^*_{s_2k_2}(2)$$

After inserting the tight binding wave function into the exchange term we get

$$\begin{aligned}M_e = \frac{1}{N^2}\sum C^{\gamma *}_{s_1'k_1'} C^{\gamma' *}_{s_2'k_2'} C^{\gamma}_{s_2k_2} C^{\gamma' *}_{s_1k_1} e^{-i(k_1'+k_2'-k_1-k_2).\vec{R}} \\ \times e^{-i(k_1'-k_2-k_2'+k_1).\frac{\vec{r}}{2}} V(R_1 - R_2)\end{aligned} \tag{2.35}$$

$$M_e = \sum \left(-i \sin \left(\frac{\varphi_{k_1'} - \varphi_{k_2}}{2} \right) \cos \left(\frac{\varphi_{k_2'} - \varphi_{k_1}}{2} \right) \right) \frac{1}{N} \delta_{k_1'+k_2'-k_1-k_2=0} \times \int \frac{d^2}{\Omega} e^{-iQ.r} V(r) \tag{2.36}$$

Substituting the direct term M_d, exchange term M_e and multiplication of the direct and exchange term $M_d M_e$ in the rate equation 2.18 we obtain

$$\begin{aligned}
\Gamma = & \frac{1}{N^2\Omega^2} \frac{8\pi}{\hbar} \\
& \times \left[\sum \cos^2 \left(\frac{\varphi_{k_1'} - \varphi_{k_1}}{2} \right) \sin^2 \left(\frac{\varphi_{k_2'} - \varphi_{k_2}}{2} \right) \delta_{(k_1'+k_2'-k_1-k_2=0)} \frac{4\pi^2 e^4}{K^2 + (k_1' - k_1)^2} \right] \\
& + \left[\sum \sin^2 \left(\frac{\varphi_{k_1'} - \varphi_{k_2}}{2} \right) \cos^2 \left(\frac{\varphi_{k_2'} - \varphi_{k_1}}{2} \right) \delta_{k_1'+k_2'-k_1-k_2=0} \frac{4\pi^2 e^4}{K^2 + (k_1' - k_2)^2} \right] \\
& + \sum \cos \left(\frac{\varphi_{k_1'} - \varphi_{k_1}}{2} \right) \sin \left(\frac{\varphi_{k_1'} - \varphi_{k_2}}{2} \right) \cos \left(\frac{\varphi_{k_2'} - \varphi_{k_1}}{2} \right) \sin \left(\frac{\varphi_{k_2'} - \varphi_{k_2}}{2} \right) \\
& \times \delta_{k_1'+k_2'-k_1-k_2=0} \frac{4\pi^2 e^4}{\sqrt{K^2 + (k_1' - k_1)^2} \sqrt{K^2 + (k_1' - k_2)^2}} \\
& \times \delta \left(\hbar\nu (|k_1'| + |k_2'| - |k_1| + |k_2|) \right)
\end{aligned} \tag{2.37}$$

Energy conservation implies

$$\hbar\nu|\vec{k}_1| + \hbar\nu|\vec{k}_2| = \hbar\nu|\vec{k}_1 + \vec{Q}| + \hbar\nu|\vec{k}_2 - \vec{Q}| \tag{2.38}$$

$$|\vec{k}_1| + |\vec{k}_2| = |\vec{k}_1 + \vec{Q}| + |\vec{k}_2 - \vec{Q}| \tag{2.39}$$

where

$$\begin{aligned}
\vec{k}_1' &= \vec{k}_1 + \vec{Q} \\
\vec{k}_2' &= \vec{k}_2 - \vec{Q}
\end{aligned} \tag{2.40}$$

For k_1, k_2, Q vectors the triangular inequalities defined as follows

$$|\vec{k}_1 + \vec{Q}| + |\vec{k}_2 - \vec{Q}| \geq |\vec{k}_1 + k_2| \geq |\vec{k}_1| - |\vec{k}_2| \tag{2.41}$$

When we use the energy conservation condition, the inequalities above become the equalities. The inequality on the left would be an equality if the vectors $\vec{k}_1 + \vec{Q}$ and $\vec{k}_2 - \vec{Q}$ indicate in the same direction. The inequality on the right would be an equality if the vectors $\vec{k}_1$ and $\vec{k}_2$ indicate in the opposite direction. If $\vec{k}_1$ and $\vec{k}_2$ indicate in the opposite direction, then the vectors $\vec{k}_1 + \vec{Q}$ and $\vec{k}_2 - \vec{Q}$ will indicate in the same direction if $\vec{k}_2$ and $\vec{Q}$ point in the same direction and $|\vec{Q}| \geq |\vec{k}_2|$ and $|\vec{k}_1| \geq |\vec{k}_2|$ and $|\vec{Q}| \leq |\vec{k}_1|$.

The Coulomb potential for graphene can be parametrized Ohno potential (onsite Coulomb interaction (cRPA)) which is equal to 9.3 eV [26]. In graphene, the effective on-site (Hubbard) interaction is (9.3 eV) in close vicinity to the critical value separating conducting graphene from an insulating phase emphasizing the importance of nonlocal Coulomb terms.

Integrating the Coulomb term in the rate equation we find

$$\int \frac{e^{-ik.r}}{\sqrt{r^2 + \delta^2}} d^2r = \frac{2\pi}{k} e^{-k\delta} \tag{2.42}$$

and if we insert this Coulomb term into the inverse-Auger process Γ we evaluate

$$\begin{aligned}\Gamma = 4 \sum_{Q,k_2} \left(2 \times \frac{4\pi^2 e^4 e^{-2Q\delta}}{Q^2} + \frac{4\pi^2 e^4 e^{-Q\delta-(k_1+k_2-Q)\delta}}{Q(k_1+k_2-Q)} \right) \\ \times \delta \left(\hbar\nu(|k_1'| + |k_2'| - |k_1| + |k_2|) \right)\end{aligned} \tag{2.43}$$

$$\begin{aligned}\Gamma = 4 \frac{A}{(2\pi)^2} \int_0^{k_1} dk_2 \int_{k_2}^{k_1} dQ \left(2 \frac{4\pi^2 e^4 e^{-2Q\delta}}{Q^2} + \frac{4\pi^2 e^4}{Q(k_1+k_2-Q)} e^{-Q\delta-(k_1+k_2-Q)\delta} \right) \\ \times \delta \left(\hbar\nu(|k_1'| + |k_2'| - |k_1| + |k_2|) \right)\end{aligned} \tag{2.44}$$

First term in the equation is the sum of M_d and $M_x$since they are equal, and second term

is the multiplication term of $M_d M_x$.

$$M_d M_x = \frac{2\pi}{\hbar}\frac{1}{N}\sum_{k_1' k_2}\frac{e^{-|k_1'-k_1|\delta}e^{-|k_1'-k_2|\delta}}{|k_1'-k_1||k_2'-k_1|}\delta(\hbar\nu_F(|k_1'|+|k_2'|-|k_1|+|k_2|)) \tag{2.45}$$

Using the definition of k_1', k_2'

$$\begin{aligned} k_1' - k_1 &= Q \\ k_2' &= k_2 - Q \end{aligned} \tag{2.46}$$

we obtain the equation for $M_d M_x$ multiplication

$$M_d M_x = \frac{2\pi}{\hbar}\frac{1}{N}\sum_{Q,k_2}\frac{e^{-|Q|\delta}e^{-|k_1+Q-k_2|\delta}}{|Q||k_2-Q-k_1|}\delta(\hbar\nu_F(|k_1'|+|k_2'|-|k_1|+|k_2|)) \tag{2.47}$$

We can evaluate the summations from one identity of the delta function

$$\delta[(k_1-k_2)^2-(k_{1'}+k_{2'})^2] = \frac{\delta(k_1-k_2-k_{1'}-k_{2'})+\delta(k_1-k_2+k_{1'}+k_{2'})}{2(k_1-k_2)} \tag{2.48}$$

where second term on the right hand side is zero. The summation over $k_{2'}$ can be eliminated by using the momentum conservation

$$\delta(k_1-k_2-k_{1'}-k_{2'}) = 2(k_1-k_2)\delta[(k_1-k_2)^2-k_{1'}^2-2k_{1'}k_{2'}-(k_1+k_2-k_{1'})^2] \tag{2.49}$$

where $k_{2'}$ is defined as

$$k_{2'} = k_1 + k_2 - k_{1'} \tag{2.50}$$

When we expand the last term in the equation 2.49 and use the momentum conservation, we evaluate the following equation

$$\delta(k_1 - k_2 - k_{1'} - k_{2'}) = \frac{(k_1 - k_2)}{2}\delta\left\{k_1 k_2 \cos^2\left[\frac{(\theta_1 - \theta_2)}{2}\right] + k_{1'}k_{2'}\sin^2\left[\frac{(\theta_{1'} - \theta_{2'})}{2}\right]\right\} \tag{2.51}$$

If we use this Dirac delta term in the rate equation we get the following equation

$$= \frac{A^2}{(2\pi)^4}\sum_{k_1}\int\int k_{1'}k_2 dk_{1'}dk_2 \int_0^{2\pi} d\theta_{1'}\int_0^{2\pi} d\theta_2 \times |M|\frac{(k_1 - k_2)}{2}\delta\left(k_1 k_2 \cos^2\left(\frac{\theta_1 - \theta_2}{2}\right) + k_{1'}k_{2'}\sin^2\left(\frac{\theta_{1'} - \theta_{2'}}{2}\right)\right) \tag{2.52}$$

To calculate the angular integral we can write the $\delta - function$ in the form of $\delta[\alpha^2 + \beta^2]$ where

$$\alpha \equiv \sqrt{k_{1'}k_{2'}}\sin\left(\frac{\theta_{1'} - \theta_{2'}}{2}\right) \tag{2.53}$$

$$\beta \equiv \sqrt{k_1 k_2}\cos\left(\frac{\theta_1 - \theta_2}{2}\right) \tag{2.54}$$

To find the θ_2' we can use the relation for k_2' equation 2.50

$$\vec{k}_{2'}^2 = (\vec{k}_1 + \vec{k}_2)^2 + \vec{k}_{1'}^2 - 2\vec{k}_{1'}.(\vec{k}_1 + \vec{k}_2) \tag{2.55}$$

$$\tan\theta_{2'} = \frac{k_1\sin\theta_1 + k_2\sin\theta_2 - k_{1'}\sin\theta_{1'}}{k_1\cos\theta_1 + k_2\cos\theta_2 - k_{1'}\cos\theta_{1'}} \tag{2.56}$$

$$(1+\tan^2\theta_{2'})\frac{\partial\theta_{2'}}{\partial\theta_{1'}} = \frac{-k_{1'}\cos\theta_{1'}}{k_1\cos\theta_1 + k_2\cos\theta_2 - k_{1'}\cos\theta_{1'}} - \frac{k_{1'}\sin\theta_{1'}(k_1\sin\theta_1 + k_2\sin\theta_2 - k_{1'}\sin\theta_{1'})}{(k_1\cos\theta_1 + k_2\cos\theta_2 - k_{1'}\cos\theta_{1'})^2} \tag{2.57}$$

Afterwards, we can form the Jacobian matris as follows

$$d\theta_{1'}d\theta_2 = J\begin{pmatrix}\theta_{1'} & \theta_2\\ \alpha & \beta\end{pmatrix}d\alpha d\beta \tag{2.58}$$

$$d\theta_{1'}d\theta_2 = \frac{d\alpha d\beta}{J\begin{pmatrix}\alpha & \beta\\ \theta_{1'} & \theta_2\end{pmatrix}} \tag{2.59}$$

By changing the $\theta_{1'}, \theta_2 \rightarrow \alpha, \beta$ a simple form for the angular integral can be obtained. The integral limits can be extended to the entire α, β plane.

$$\int_{-\infty}^{\infty}\frac{d\alpha}{|\partial\alpha/\partial\theta_{1'}|}\int_{-\infty}^{\infty}\frac{d\beta}{|\partial\beta/\partial\theta_2|}\delta[\alpha^2+\beta^2] \tag{2.60}$$

Transforming the Cartesian coordinates α, β into the polar coordinates ρ, φ yields

$$\int_0^{2\pi}\frac{d\varphi}{|\partial\beta/\partial\theta_2|}\int_0^{\infty}\frac{\rho d\rho}{|\partial\alpha/\partial\theta_{1'}|}\delta(\rho^2) = \frac{1}{2}\int_0^{2\pi}\frac{d\varphi}{|\partial\beta/\partial\theta_2|}\int_0^{\infty}\frac{\rho d\rho}{|\partial\alpha/\partial\theta_{1'}|}\delta(\rho) \tag{2.61}$$

where

$$2\rho\delta(\rho^2) = \delta(\rho) \tag{2.62}$$

$\alpha = 0, \beta = 0$ is equivalent to $\theta_1 = \theta_2 + \pi, \theta_{1'} = \theta_{2'}$ respectively. After substituting the equations obtained above in the rate equation, we can write the final form of the generation rate equation

$$\Gamma = \frac{2\pi}{\hbar}\frac{1}{N_{el}}e^4\frac{1}{\hbar\nu_F}\int_0^{k_1} dk_2 \int_0^{k_1-k_2} dk_{1'}\frac{e^{(-2Q\delta)}}{Q^2}|M|^2$$
$$\times\left[f(k_2)\right]\left[1-f(k_{1'})\right]\left[1-f(k_{2'})\right]\frac{k_1k_2k_{2'}}{4\sqrt{k_{1'}k_{2'}k_1k_2}} \tag{2.63}$$

Another way of solving $\delta - function$ is to use the Taylor expansion method. Considering the Dirac Delta function as a function 'f' and expanding the terms in the Dirac Delta function in terms of x and y components we get

$$f = \delta(|k_1+Q| + |k_2-Q| - |k_1| + |k_2|) = \sqrt{(k_{1x}+Q_x)^2+Q_y^2}$$
$$+\sqrt{(k_{2x}-Q_x)^2+(k_{2y}-Q_y)^2} - k_1 + k_2 \tag{2.64}$$

$$\left.\frac{\partial^2 f}{\partial Q_y^2}\right|_{root} = \frac{1}{k_{1'}} + \frac{1}{k_{2'}} \tag{2.65}$$

$$\left.\frac{\partial^2 f}{\partial k_{2y}^2}\right|_{root} = \frac{1}{k_{2'}} + \frac{1}{k_2} \tag{2.66}$$

$$\frac{\partial^2 f}{\partial k_{2y}\partial Q_y} = -\frac{1}{k_{2'}} + \frac{(k_{2y}-Q_y)^2}{k_{2'}^3} \tag{2.67}$$

$$\left.\frac{\partial^2 f}{\partial k_{2y}\partial Q_y}\right|_{root} = -\frac{1}{k_{2'}} \tag{2.68}$$

After finding the all term we can write funtion f as follows

$$f(k_2, Q) = \frac{1}{2}\left(\frac{1}{k_{1'}} + \frac{1}{k_{2'}}\right) Q_y^2 + \frac{1}{2}\left(\frac{1}{k_{2'}} + \frac{1}{k_2}\right) k_{2y}^2 + \left(-\frac{1}{k_{2'}}\right) k_{2y} Q_y \tag{2.69}$$

If we write Eq. 2.69 in the form of matrix we get

$$\begin{pmatrix} Q_y & k_{2y} \end{pmatrix} \begin{pmatrix} \frac{1}{k_{1'}} + \frac{1}{k_{2'}} & -\frac{1}{2k_{2'}} \\ -\frac{1}{2k_{2'}} & \frac{1}{k_{2'}} + \frac{1}{k_2} \end{pmatrix} \begin{pmatrix} Q_y \\ k_{2y} \end{pmatrix} \tag{2.70}$$

Transforming the Q_y, k_{2y} into χ_+, χ_-

$$dQ_y dk_{2y} = \begin{pmatrix} \frac{\partial Q_y}{\partial \chi_+} & \frac{\partial Q_y}{\partial \chi_-} \\ \frac{\partial k_{2y}}{\partial \chi_+} & \frac{\partial k_{2y}}{\partial \chi_-} \end{pmatrix} d\chi_+ d\chi_- \tag{2.71}$$

where

$$\begin{aligned} \chi_+ &= (\lambda_+)_1 Q_y + (\lambda_+)_2 k_2 y \\ \chi_- &= (\lambda_-)_1 Q_y + (\lambda_-)_2 k_2 y \end{aligned} \tag{2.72}$$

and $\lambda_\pm$ is defined as

$$|\lambda_\pm\rangle = \frac{1}{\sqrt{\left(-\frac{1}{k_2'}\right)^2 + \left(2\left(\frac{1}{k_2} + \frac{1}{k_2'}\right) \pm \sqrt{\left(\frac{1}{k_2'}\right)^2 + \left(\frac{1}{k_1'} + \frac{1}{k_2'} - \frac{1}{k_2} - \frac{1}{k_2'}\right)^2}\right)^2}} \begin{pmatrix} -\frac{1}{k_2'} \\ 2\left(\frac{1}{k_2} + \frac{1}{k_2'}\right) \pm \sqrt{\left(\frac{1}{k_2'}\right)^2 + \left(\frac{1}{k_1'} + \frac{1}{k_2'} - \frac{1}{k_2} - \frac{1}{k_2'}\right)^2} \end{pmatrix} \tag{2.73}$$

$$\begin{pmatrix} Q_y & k_{2y} \end{pmatrix} U^{\dagger} \begin{pmatrix} \lambda_+ & 0 \\ 0 & \lambda_- \end{pmatrix} U \begin{pmatrix} Q_y \\ k_{2y} \end{pmatrix} \tag{2.74}$$

where U is the unitary matrix.

$$\begin{aligned} U^{\dagger}U &= 1 \\ detU^{\dagger} = detU &= \pm 1 \end{aligned} \tag{2.75}$$

After some calculations, the integral term can be obtained as below

$$\begin{aligned} \int dQ_y dk_{2y} &= \int \frac{d\chi_+ d\chi_-}{detU} \delta(\lambda_+ \chi_+^2 + \lambda_- \chi_-^2) \\ &= \int \frac{d\chi'_+ d\chi'_-}{\sqrt{\lambda_+ \lambda_-}} \delta(\chi_+'^2 + \chi_-'^2) \end{aligned} \tag{2.76}$$

Changing the coordinate system we obtain

$$\int \frac{2\pi\rho d\rho \delta(\rho^2)}{\sqrt{\lambda_+ \lambda_-}} = \int \frac{\pi dy \delta(y)}{\sqrt{\lambda_+ \lambda_-}} = \frac{\pi}{\sqrt{\lambda_+ \lambda_-}} = \frac{\pi \sqrt{4k'_1 k'_2} k_2}{\sqrt{k'_1 + k_2 + k'_2}} \tag{2.77}$$

Since the $\vec{k}_2$ is in the opposite direction with the k'_1, k'_2 we get the final form of the integral as follows

$$= \frac{\pi \sqrt{4k'_1 k'_2 k_2}}{\sqrt{k_1}} \tag{2.78}$$

Using two different methods to solve the Dirac Delta we obtain the same Jacobian expression in the equations 2.63 and 2.78. Although these results mathematically coincides with Eq.(24) of [27] and Eq.(7) of [28] there are different results from Eq.(14) of [8] and Eq.(A.13) of [29].

The order of the generation rate can be calculated by using Eq. 2.63

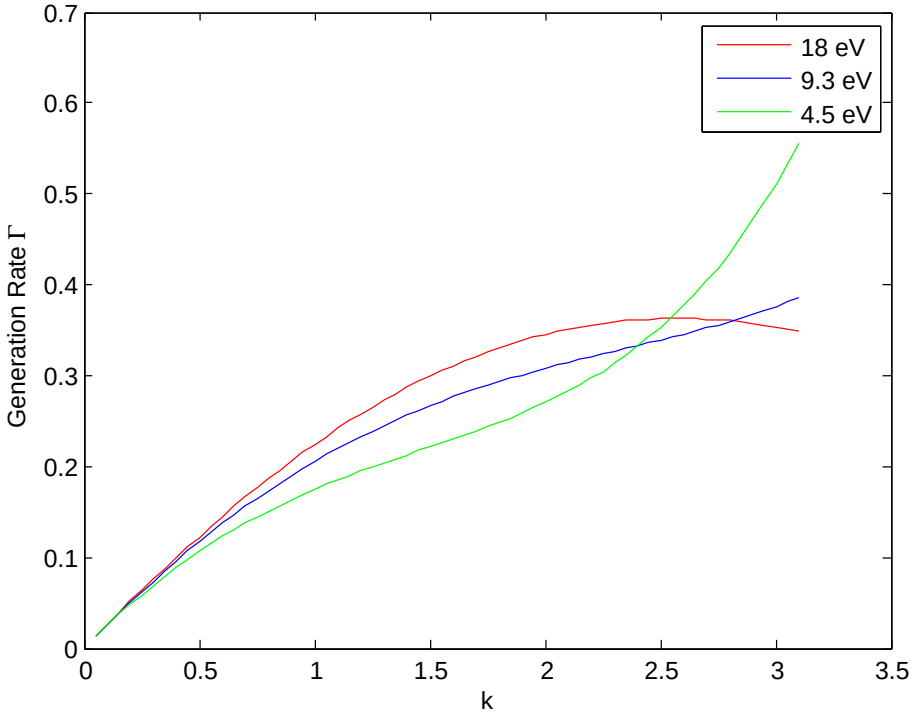

Figure 2.3. Generation rate versus k for lattice constant parameter according to Bohr radius $(0.54\mathring{A})$. $\delta = 0.31\mathring{A}$ (red line), $\delta = 0.61\mathring{A}$ (blue line), $\delta = 1.22\mathring{A}$ (green line) where on-site Coulomb interaction is given as $U = \frac{e^2}{\delta}$

$$\Gamma = \frac{2\pi}{\hbar} \frac{e^4}{N_{el}\hbar v_F} \frac{1}{a} I \tag{2.79}$$

$$\Gamma = \frac{2\pi}{\hbar} \frac{\left(\frac{e^2}{a}\right)^2}{N_{el}\hbar v_F \frac{1}{a}} I \tag{2.80}$$

We can use the following parameters to evaluate the order of magnitude: $v_F = \frac{3}{2}\frac{ta}{\hbar}$, $\delta = 0.61\mathring{A}$, lattice constant of graphene $a = 2.46\mathring{A}$, $\frac{e^2}{a_0} = 27.2eV$, hopping parameter $t = 2.8eV$ and on-site Coulomb interaction is given as $U = \frac{e^2}{\delta}$. Finally, we get the generation rate at the order of

$$\Gamma \propto \frac{1}{\hbar} \frac{\left(\frac{e^2}{a}\right)^2}{N_{el}t} \approx 10^{17} s^{-1} \tag{2.81}$$

2.2.2. Intervalley Scattering

In this part, we calculate the intervalley process in graphene. We take into consideration only the electron-electron scattering mechanism. For intervalley scattering, using the phonon scattering the generation rate have been done by F.Rana [32]. There are two cases for intervalley scattering: First case is k_1, k_1' in the K valley and k_2, k_2' in the K' valley. In this case, we can write the direct scattering $k_1 \rightarrow k_1'$ and $k_2 \rightarrow k_2'$ and the exchange scattering $k_1 \rightarrow k_2'$ and $k_2 \rightarrow k_1'$ respectively. Therefore in the exchange scattering we obtain a extra term $\Delta k = K' - K$. Second case is k_1, k_2' in the K valley and k_2, k_1' in the K' valley. In this case, we can write the direct scattering $k_1 \rightarrow k_1'$ and $k_2 \rightarrow k_2'$ and the exchange scattering $k_1 \rightarrow k_2'$ and $k_2 \rightarrow k_1'$ respectively. In this situation, we obtain a extra term $\Delta k = K' - K$ in the direct scattering. We know that direct scattering wave vectors

$$\begin{aligned} \vec{k_1'} &= \vec{k_1} + \vec{Q} \\ \vec{k_2'} &= \vec{k_2} - \vec{Q} \end{aligned} \tag{2.82}$$

and exchange scattering wave vectors

$$\begin{aligned} \vec{k_2'} &= \vec{k_1} + \vec{Q} \\ \vec{k_1'} &= \vec{k_2} - \vec{Q} \end{aligned} \tag{2.83}$$

If we define the wave vectors k_1, k_2, k_1', k_2' for the intervalley scattering we evaluate

$$\begin{aligned} \vec{k_1} &= \vec{K} + \tilde{k_1} \\ \vec{k_2} &= \vec{K'} + \tilde{k_2} \\ \vec{k_2'} &= K' + \tilde{k_2'} \\ \vec{k_1'} &= K + \tilde{k_1'} \end{aligned} \tag{2.84}$$

If we define the K' wave vectors as $\tilde{k_1}, \tilde{k_2}$ we obtain the momentum transfer as follows

$$\begin{aligned} \tilde{k_1'} &= \tilde{k_1} + \vec{Q} \\ \tilde{k_2'} &= \tilde{k_2} - \vec{Q} \end{aligned} \tag{2.85}$$

$$\tilde{k_1} + \tilde{k_2} = \tilde{k_1'} + \tilde{k_2'} \tag{2.86}$$

$$\begin{aligned} \vec{Q} &\rightarrow \vec{Q} + \Delta k \\ \Delta k &= K' - K \end{aligned} \tag{2.87}$$

$$\begin{aligned} \vec{k}_{1'} &= \vec{k}_1 + Q + \Delta k = K' + \tilde{k}_1 + Q \\ \vec{k}_{2'} &= \vec{k}_2 - Q - \Delta k = K' + \tilde{k}_2 - Q \end{aligned} \tag{2.88}$$

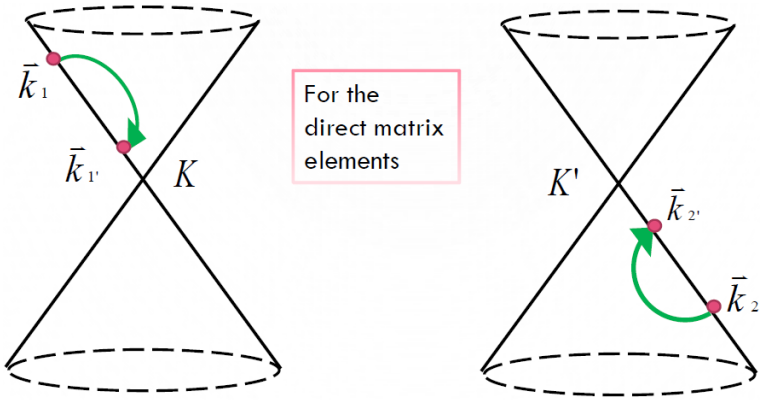

Figure 2.4. 1. Case: $\vec{k}_1$ and $\vec{k}_{1'}$ are in the K valley and $\vec{k}_2$ and $\vec{k}_{2'}$ are in the K' valley

We can write the inverse-Auger rate matrix elements for two states in the interval-

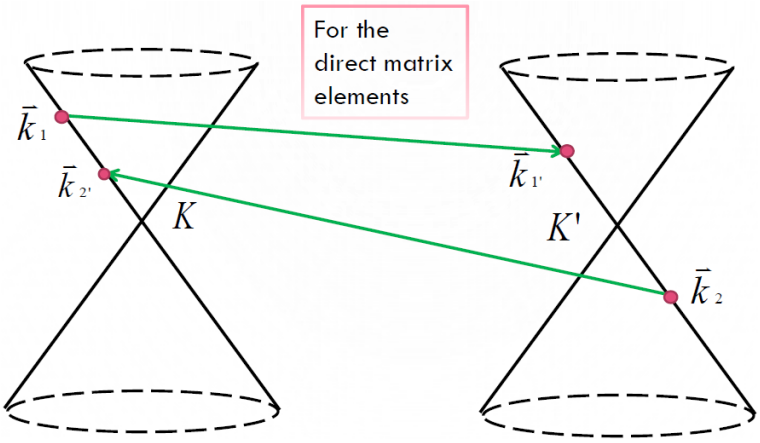

Figure 2.5. 2. Case : $\vec{k}_1$ and $\vec{k}_{2'}$ are in the K valley and $\vec{k}_2$ and $\vec{k}_{1'}$ are in the K' valley

ley scattering: 1) k_1 and k_2 are both in the same state and 2) k_1 and k_2 are in the different state.

1) k_1 and k_2 are in the same state:

$$\Gamma = \frac{2\pi}{\hbar} \sum_{k_1', k_2'} \frac{1}{4} |M_d - M_e|^2 \delta(\hbar\nu(|\tilde{k_{1'}}| + |\tilde{k_2'}| - |\tilde{k_1}| + |\tilde{k_2}|)) \tag{2.89}$$

2) k_1 and k_2 in the different state:

$$\Gamma = \frac{2\pi}{\hbar} \sum_{k_1', k_2'} \left(\frac{1}{4} |M_d|^2 + \frac{1}{4} |M_e|^2 \right) \delta(\hbar\nu(|\tilde{k_{1'}}| + |\tilde{k_2'}| - |\tilde{k_1}| + |\tilde{k_2}|)) \tag{2.90}$$

Two different cases can be written for the intervalley scattering (k_1 and k_2 in the different valley). Firsty, If k_1, k_1' are in the K valley and k_2, k_2' are in the K' valley the rate can be written as

$$\begin{aligned} \Gamma_1 = & \frac{2\pi}{\hbar} \frac{1}{N_{el}} e^4 \frac{1}{\hbar\nu_F} \int dQ \int dk_2 \left(\frac{e^{-2Q\delta}}{|Q|^2} \right) \frac{k_1 k_2 k_{2'}}{4\sqrt{k_{1'} k_{2'} k_1 k_2}} \\ & + \frac{2\pi}{\hbar} \frac{1}{N_{el}} e^4 \frac{1}{\hbar\nu_F} \int dQ \int dk_2 \left(\frac{e^{-2(\Delta k + Q)\delta}}{|\Delta k + Q|^2} \right) \frac{k_1 k_2 k_{2'}}{4\sqrt{k_{1'} k_{2'} k_1 k_2}} \end{aligned} \tag{2.91}$$

Secondly, If k_1 is in the K valley and k_1' is in the K' valley and k_2 is in the K' valley and

k_2' is in the K valley the rate can be written as

$$\Gamma_2 = -\frac{2\pi}{\hbar}\frac{1}{N_{el}}e^4\frac{1}{\hbar\nu_F}\int dQ\int dk_2\frac{e^{-Q\delta}}{|Q|}\frac{e^{-(\tilde{k_2}-\tilde{k_1}-\vec{Q}+\Delta k)\delta}}{|\tilde{k_2}-\tilde{k_1}-Q+\Delta k|}\frac{\tilde{k_1}\tilde{k_2}\tilde{k_{2'}}}{4\sqrt{\tilde{k_{1'}}\tilde{k_{2'}}\tilde{k_1}\tilde{k_2}}}$$
$$+\frac{2\pi}{\hbar}\frac{1}{N_{el}}e^4\frac{1}{\hbar\nu_F}\int dQ\int dk_2\frac{e^{-(Q+\Delta k)\delta}}{|Q+\Delta k|}\frac{e^{-(\tilde{k_2}-\tilde{k_1}-\vec{Q})\delta}}{|\tilde{k_2}-\tilde{k_1}-Q|}\frac{\tilde{k_1}\tilde{k_2}\tilde{k_{2'}}}{4\sqrt{\tilde{k_{1'}}\tilde{k_{2'}}\tilde{k_1}\tilde{k_2}}} \tag{2.92}$$

Finally, the total rate can be written as the sum of the intravalley and intervalley processes:

$$\Gamma_{Total} = \Gamma_1 + \Gamma_2 + \Gamma_{intravalley} \tag{2.93}$$

CHAPTER 3

INVERSE-AUGER EFFECT IN ARMCHAIR NANORIBBONS

3.1. Graphene Nanoribbons

Graphene nanoribbons are obtained by using graphene sheets in the form of quasi 1D wire along a given direction. Graphene nanoribbons consist of graphene with a finite with and infinite length so the unit cell of the nanoribbon has 2N carbon atoms. Since the carbon atoms localized at the edges, the electronic and magnetic properties of a graphene nanoribbon can be different from the bulk graphene. The simplest types of nanoribbon geometries are armchair and zigzag edge shapes. The edge carbon atoms in armchair and zigzag nanoribbons, have two σ bonds and one π bond. The remaining dangling σ bonds are passivated by H atoms. Graphene systems such as clusters, or nanoribbons with zigzag edge localize edge states at the Fermi energy. The density of states near the Fermi energy is singular for zigzag nanoribbons and a flat energy band appears around the Fermi energy from the K to M points for zigzag nanoribbons. Armchair nanoribbons do not show zero energy states and the Fermi energy is usually set to zero. No edge states appear for armchair nanoribbons. In the armchair nanoribbons, the energy gap oscillates as a function of N, and for $N = 3r - 1$ the armchair nanoribbons are metallic, being semiconducting otherwise. In the zigzag nanoribbon, the unit cell contains A-type atoms that change along the unit cell with B-type atoms. Zigzag nanoribbons may have axial symmetry or may not. In armchair nanoribbons, the edges consists of a line of A-B dimers.

Graphene nanoribbons are sensitive to their surrounding conditions, which provides a route for regulating their electronic properties. In addition, other factors such as the presence of strain, finite size effect and edge effect can be used to tune the electronic properties of graphene nanoribbons. Armchair nanoribbons having a tunable band gap are alternative structures for optoelectronic devices. The performance of optoelectronic devices depends on the carrier generation and recombination rates.

3.2. The Electronic Structure of Armchair Nanoribbons

In this section, we obtain the energy spectrum and wave function by using the analytical solution of the nearest-neighbor tight-binding model.[30]

The tight-binding Hamiltonian for electrons in armchair nanoribbons can be written as

$$H = -t\sum_{\ell}\left[\sum_{m\epsilon odd} a_{\ell}^{\dagger}(m)b_{\ell-1}(m) + \sum_{m\epsilon even} a_{\ell}^{\dagger}(m)b_{\ell}(m)\right] + h.c. \tag{3.1}$$

$$-t\sum_{\ell}\sum_{m=1}^{N-1}\left[b_{\ell}^{\dagger}(m+1)a_{\ell}(m) + a_{\ell}^{\dagger}(m+1)b_{\ell}(m)\right] + h.c. \tag{3.2}$$

where $a_{\ell}^{\dagger}(m)(a_{\ell}(m))$ and $b_{\ell}^{\dagger}(m)(b_{\ell}(m))$ create (annihilate) an electron on sublattices A and B in the ℓth unit cell, respectively. The longitudinal hopping of electrons are described by the first line in the Hamiltonian, and the transverse hopping is described by the second line. The anticommutation relations for the operators is written as:

$$\{a_{\ell}(m), a_{\ell}^{\dagger}(m')\} = \delta_{\ell,\ell'}\delta_{m,m'} \tag{3.3}$$

$$\{b_{\ell}(m), b_{\ell}^{\dagger}(m')\} = \delta_{\ell,\ell'}\delta_{m,m'} \tag{3.4}$$

and other anticommutations are zero. If we assume that the system has L unit cells, the periodic boundary condition satisfy

$$a_{\ell+L}(m) = a_{\ell}(m) \tag{3.5}$$

$$b_{\ell+L}(m) = b_{\ell}(m) \tag{3.6}$$

The Fourier transformation of the tight-binding Hamiltonian is ,

$$a_{\ell}(m) = \frac{1}{\sqrt{L}}\sum_{k} e^{iky_{\ell,mA}}\alpha_k(m) \tag{3.7}$$

$$b_{\ell}(m) = \frac{1}{\sqrt{L}}\sum_{k} e^{iky_{\ell,mB}}\beta_k(m) \tag{3.8}$$

where yl,mA (yl,mB) is the y-coordinate of the mA (mB) site in the lth unit cell.

The longitudinal wavenumber k is given by

$$k = \frac{2\pi}{L}m \tag{3.9}$$

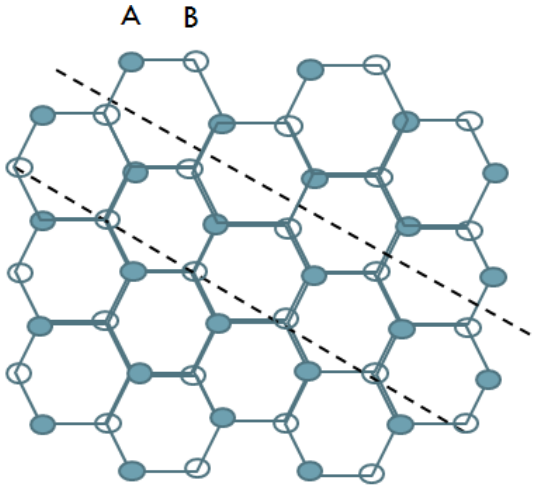

Figure 3.1. Structure of the armchair ribbon.

$$m = 0, \pm 1, \pm 2, \ldots, \pm\frac{L}{2} - 1, \frac{L}{2} \tag{3.10}$$

$$-\pi \leq k \leq \pi \tag{3.11}$$

The wave function for the lattice can be defined in the form of

$$|\Psi(k)\rangle = \sum_m (\psi_{m,A}\alpha_k^\dagger(m) + \psi_{m,B}\beta_k^\dagger(m))|0\rangle \tag{3.12}$$

$$\alpha_k(m)|0\rangle = \beta_k(m)|0\rangle \tag{3.13}$$

where $\psi_{m,A}(\psi_{m,B})$ is a probability amplitude and $|0\rangle$ is a vacuum state. Substituting the tight-binding Hamiltonian described above and this one-particle state into the Schrödinger equation

$$H|\Psi(k)\rangle = E|\Psi(k)\rangle \tag{3.14}$$

and calculating the matrix elements $< 0|a_\ell(m)Ha_\ell^\dagger(m)|0 >$ and $< 0|b_\ell(m)Hb_\ell^\dagger(m)|0 >$ with use of commutation relation we obtain the following set of equations of motion:

$$E\psi_{m,A} = -e^{-ik}\psi_{m,B} - \psi_{m-1,B} - \psi_{m+1,B} \tag{3.15}$$

$$E\psi_{m,B} = -e^{+ik}\psi_{m,A} - \psi_{m-1,a} - \psi_{m+1,A} \tag{3.16}$$

$$m = 1, 2, \ldots, N \tag{3.17}$$

Using the transfer matrix method we obtain the recurrence equation.([31])

$$-E\begin{pmatrix}\psi_A^m\\ \psi_B^m\end{pmatrix}=\begin{pmatrix}0 & 1\\ 1 & 0\end{pmatrix}\begin{pmatrix}\psi_A^m\\ \psi_B^m\end{pmatrix}+\begin{pmatrix}0 & e^{-ik}\\ 1 & 0\end{pmatrix}\begin{pmatrix}\psi_A^{m-1}\\ \psi_B^{m-1}\end{pmatrix}+\begin{pmatrix}0 & 1\\ e^{+ik} & 0\end{pmatrix}\begin{pmatrix}\psi_A^{m+1}\\ \psi_B^{m+1}\end{pmatrix} \quad (3.18)$$

m changes from $J=2$ to $m=N-1$. For $m=1$ and $m=N$ we can write recurrence equation,

$$-E\begin{pmatrix}\psi_A^1\\ \psi_B^1\end{pmatrix}=\begin{pmatrix}0 & 1\\ 1 & 0\end{pmatrix}\begin{pmatrix}\psi_A^1\\ \psi_B^1\end{pmatrix}+\begin{pmatrix}0 & 1\\ e^{+ik} & 0\end{pmatrix}\begin{pmatrix}\psi_A^2\\ \psi_B^2\end{pmatrix} \quad (3.19)$$

$$-E\begin{pmatrix}\psi_A^N\\ \psi_B^N\end{pmatrix}=\begin{pmatrix}0 & 1\\ 1 & 0\end{pmatrix}\begin{pmatrix}\psi_A^N\\ \psi_B^N\end{pmatrix}+\begin{pmatrix}0 & e^{-ik}\\ 1 & 0\end{pmatrix}\begin{pmatrix}\psi_A^{N-1}\\ \psi_B^{N-1}\end{pmatrix} \quad (3.20)$$

For $m=1$ and $m=N$ the boundary condition satisfies

$$\begin{pmatrix}\psi_A^0\\ \psi_B^0\end{pmatrix}=0 \quad (3.21)$$

By using the following matrices

$$K=\begin{pmatrix}E & 1\\ 1 & E\end{pmatrix} \quad (3.22)$$

$$T=\begin{pmatrix}0 & 1\\ z & 0\end{pmatrix} \quad (3.23)$$

$$T^{-1}=\begin{pmatrix}0 & z^*\\ 1 & 0\end{pmatrix} \quad (3.24)$$

we can rewrite the recurrence equations.Here, z is defined as $z=e^{+ik}$, $z^*=e^{-ik}$

$$T\psi^{m+1}+K\psi^m+T^{-1}\psi^{m-1}=0 \quad (3.25)$$

$$\psi^m\equiv^t(\psi_A^m,\psi_B^m) \quad (3.26)$$

By introducing the matrix U, the recurrence equation can be diagonalized

$$\phi^{m+1}+U^{-1}T^{-1}KU\phi^{m-1}=0 \quad (3.27)$$

where $\phi^m \equiv U^{-1}\psi^m$ The characteristic equation is written as

$$\begin{aligned} x^2 + \lambda_+ x + \frac{1}{z} &= 0 \\ \leftrightarrow (x - w_+^{-1}e^{ip})(x - w_+^{-1}e^{-ip}) &= 0 \end{aligned} \tag{3.28}$$

where $w_+ = e^{\frac{ik}{2}}$, $w_- = -e^{\frac{ik}{2}}$ and p is defined as $2cosp \equiv -w_+\lambda_+$

$$2cosp \equiv -\frac{w_+^{-1} + \sqrt{z + z^* - 2 + 4E^2}}{2} \tag{3.29}$$

The following equations are the eigenvalues and the eigen spinors of the $T^{-1}K$ matrix

$$\lambda_\pm = \frac{1 + z \pm \sqrt{(-1+z)^2 + 4zE^2}}{2zE} \tag{3.30}$$

$$\psi_\pm = \begin{pmatrix} \frac{1+z\pm\sqrt{(-1+z)^2+4zE^2}}{2zE} \\ 1 \end{pmatrix} \tag{3.31}$$

$$H(k) = \begin{pmatrix} h_{AA}(k) & h_{AB}(k) \\ h_{BA}(k) & h_{BB}(k) \end{pmatrix} \tag{3.32}$$

In armchair nanoribbons, there is no electron hopping between same sublattices.

$$h_{AA}(k) = h_{BB}(k) = 0 \tag{3.33}$$

The tridiagonal matrix $h_{AB}(k)$ is given by

$$h_{AB}(k) = \begin{pmatrix} 1 & e^{-ik} & 0 & \dots & \dots & 0 \\ 1 & 1 & e^{-ik} & 0 & \dots & 0 \\ 0 & 1 & 1 & e^{-ik} & \dots & 0 \\ \vdots & & \ddots & \ddots & \ddots & \vdots \\ \vdots & & 0 & 1 & 1 & e^{-ik} \\ 0 & \dots & \dots & 0 & 1 & 1 \end{pmatrix} \tag{3.34}$$

$h_{BA}(k)$ is Hermitian conjugate of $h_{AB}(k)$,i.e.,

$$h_{BA}(k) = h^{\dagger}_{AB}(k) \tag{3.35}$$

Since the 0B, 0A, (N + 1)A and (N +1)B sites are missing, the equations of motion are modified at the armchair edge to

$$E\psi_{1,A} = -e^{ik/2}\psi_{1,B} - \psi_{2,B} \tag{3.36}$$

$$E\psi_{1,B} = -e^{-ik/2}\psi_{1,A} - \psi_{2,A} \tag{3.37}$$

$$E\psi_{N,A} = -e^{ik/2}\psi_{m,A} - \psi_{N-1,B} \tag{3.38}$$

$$E\psi_{N,A} = -e^{-ik/2}\psi_{N,a} - \psi_{N-1,A} \tag{3.39}$$

Thus, we assume the boundary condition for armchair nanoribbons as

$$\psi_{0,A} = \psi_{0,B} = \psi_{N+1,A} = \psi_{N+1,B} = 0 \tag{3.40}$$

$$\begin{pmatrix} E & \epsilon_p + e^{ik/2} \\ \epsilon_p + e^{-ik/2} & E \end{pmatrix} \begin{pmatrix} A \\ C \end{pmatrix} = 0 \tag{3.41}$$

$$\epsilon_p = 2cos(p) \tag{3.42}$$

$$E_{\pm} = \pm\sqrt{1 + 4cospcos(k/2) + 4cosp^2} \tag{3.43}$$

$$p = \frac{r}{N+1}\pi, r = 1, 2, 3...N \tag{3.44}$$

$$E_{\pm} = 0, k = 0, N = 3r - 1(r = 1, 2, ...) \tag{3.45}$$

which is the condition for metallic armchair nanoribbons. The wavefunction is written as

$$\begin{pmatrix} \psi_{m,A} \\ \psi_{m,B} \end{pmatrix} = M \begin{pmatrix} \mp\sqrt{\epsilon_p + e^{-ik/2}} \\ \sqrt{\epsilon_p + e^{ik/2}} \end{pmatrix} \times Sin(mp) \tag{3.46}$$

Here M is the normalization constant, which satisfies the equation

$$\sum_{m=1}^{N}(|\psi_{m,A}|^2 + |\psi_{m,B}|^2) = 1 \tag{3.47}$$

$$M^2 = \frac{1}{2|E|}(\sum_{m=1}^{N} sin^2(mp))^{-1} \tag{3.48}$$

$$M = \frac{1}{\sqrt{E}}(N - \frac{sin(Np)}{sin(p)}cos[(N+1)p])^{-1} \tag{3.49}$$

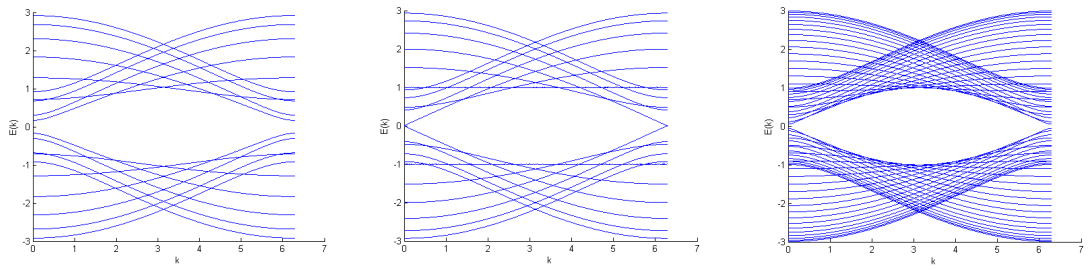

Figure 3.2. Energy band diagrams of armchair nanoribbon for N=10, N=11, N=30 respectively.

3.3. Inverse Auger Rate Calculation in Nanoribbons

In this part we have calculated the inverse auger rate for armchair nanoribbons by using the tight binding method. The tight binding wave function for armchair nanoribbon can be written as

$$\phi^{\gamma}_{sk} = \frac{1}{N_x}\sum C^{\gamma}_{sk}\chi(\vec{r} - na\widehat{x} - \ell_{\gamma})e^{ikna} \tag{3.50}$$

where $\vec{R}$ is in the x direction.

$$\vec{R} = na\widehat{x} \tag{3.51}$$

$$\chi^{\gamma}(\vec{r} - \vec{R}) = \chi(\vec{r} - \vec{R} - \vec{\ell}_{\gamma}) \tag{3.52}$$

By using the this wave function the direct term of the matrix elements is written as

$$M_d = \frac{1}{N^2}\int d^2r_1 d^2r_2 C^{\gamma *}_{s'_1 k'_1} C^{\gamma}_{s_1 k_1} |\chi^{\gamma}(r_1 - R)|^2 e^{-i(k'_1 - k_1)na} V(r_1 - r_2)$$
$$C^{\gamma' *}_{s'_2 k'_2} C^{\gamma'}_{s_2 k_2} |\chi^{\gamma'}(r_2 - R')|^2 e^{-i(k'_2 - k_2)n'a} \tag{3.53}$$

$$M_d = \frac{1}{N^2}\int d^2r_1 d^2r_2 C^{\gamma *}_{s'_1 k'_1} C^{\gamma}_{s_1 k_1} |\chi^{\gamma}(r_1 - R)|^2 e^{-i(k'_1 - k_1)na} V(r_1 - r_2)$$
$$C^{\gamma' *}_{s'_2 k'_2} C^{\gamma'}_{s_2 k_2} |\chi^{\gamma'}(r_2 - R')|^2 e^{-i(k'_2 - k_2)n'a} \tag{3.54}$$

If we define $\vec{r} = x\hat{x}$ then coulomb term $V(\vec{R} + \ell_\gamma - \vec{R'} - \ell_{\gamma'})$ written as $V(x\hat{x} + \ell_\gamma - \ell_{\gamma'\lambda})$

$$M_d = \frac{1}{N^2}\int d^2r_1 d^2r_2 C^{\gamma *}_{s'_1 k'_1} C^{\gamma}_{s_1 k_1} C^{\gamma' *}_{s'_2 k'_2} C^{\gamma'}_{s_2 k_2} N\delta_{\sum k_i = 0} \int \frac{dx}{a} e^{-iQx} V_x \tag{3.55}$$

where index $i = 1, 2$. The conservation of the momentum follows from the Kronecker delta $\delta_{\sum k_i = 0}$

$$M_d = \frac{1}{N^2}\int d^2r_1 d^2r_2 C^{\gamma *}_{s'_1 k'_1} C^{\gamma}_{s_1 k_1} C^{\gamma' *}_{s'_2 k'_2} C^{\gamma'}_{s_2 k_2}$$
$$\times N\delta_{\sum k_i = 0} e^{-iQx} \int \frac{dx}{a} \frac{1}{\sqrt{x^2 + 2x(\ell_\gamma - \ell_{\gamma'})_x + (\ell_\gamma - \ell_{\gamma'})^2}} \tag{3.56}$$

$$\int_\infty^\infty \frac{dx}{a} e^{-iQx} \frac{1}{\sqrt{x^2 + 2x(\ell_\gamma - \ell_{\gamma'})_x + (\ell_\gamma - \ell_{\gamma'})_y^2}} \tag{3.57}$$

$$\delta^2 = (\ell_\gamma - \ell_{\gamma'})_y^2 + \delta_0^2 \tag{3.58}$$

Integral of the Coulomb term is found from Mathematica

$$\int_{-\infty}^{\infty} \frac{1}{\sqrt{x^2 + \delta^2}} e^{-iQx} = \int_{-\infty}^{\infty} dx \frac{1}{\sqrt{x^2 + 1}} e^{-iQ\delta x} = 2K_0(|Q|\delta) \tag{3.59}$$

$x \to x\delta$

where K_0 is the Bessel function.

$$M_d = \frac{1}{N} C^{*\gamma}_{ck'_1} C^{\gamma}_{ck_1} C^{*\gamma}_{ck'_2} C^{\gamma}_{vk_2} \delta_{\sum_{k_i - k'_i = 0}} \frac{e^2}{a} 2K_0(|Q|\delta) e^{-iQ.(\ell_\gamma - \ell_{\gamma'})_x} \tag{3.60}$$

Exchange term of the matrix elements is expressed

$$M_e = \frac{1}{N^2}\sum \int d^2r_1 d_2^2 C^{*\gamma}_{s_1'k_1'} C^{\gamma}_{s_2k_2} |\chi^{\gamma}(r_1 - R)|^2 V(r_1 - r_2) \\ \times C^{*\gamma}_{s_2'k_2'} C^{\gamma}_{s_1k_1} |\chi^{\gamma'}(r_2 - R')|^2 e^{-i(k_1'-k_2).r_1 - i(k_2'-k_1).r_2} \tag{3.61}$$

Momentum transfer for exchange term is defined as

$$Q = k_1' - k_2 \tag{3.62}$$

$$M_e = \frac{1}{N^2}\sum C^{*\gamma}_{k_1's_1'} C^{\gamma}_{k_2s_2} C^{*\gamma'}_{k_2's_2'} C^{\gamma'}_{k_1s1} V(R_1 + \ell_\gamma - R_2 - \ell_{\gamma'})_x e^{-i(k_1'+k_2'-k_1-k_2).R} e^{-iQ.r} \tag{3.63}$$

$$M_e = \frac{1}{N}\sum C^{*\gamma}_{k_1's_1'} C^{\gamma}_{k_2s_2} C^{*\gamma'}_{k_2's_2'} C^{\gamma'}_{k_1s1} \delta_{\sum_{k_i'} - \sum_{k_i}=0} \sum_r e^{-iQ.r} V(R_1 - R_2 + \ell_\gamma - \ell_{\gamma'}) \tag{3.64}$$

$$\sum_r e^{-iQr} \to \int \frac{dx}{a} e^{-iQx} \tag{3.65}$$

Therefore, final form of exchange term is

$$M_e = \frac{1}{N}\sum C^{*\gamma}_{ck_1'} C^{\gamma}_{vk_2} C^{*\gamma'}_{ck_2'} C^{\gamma'}_{ck_1} \delta_{\sum_{ki'-ki=0}} \frac{e^2}{a} 2K_0(|Q|\delta) e^{-iQ(\ell_\gamma - \ell_{\gamma'})_x} \tag{3.66}$$

Finally, we can write the total rate

$$\Gamma = 4^2 \frac{2\pi}{\hbar} \frac{1}{N_{el}^2} \left(\frac{e^2}{a}\right)^2 \left[\sum_{Q,k_2} |\sum_{\gamma} C^{*\gamma}_{ck'_1} C^{\gamma}_{ck_1} e^{-iQ\ell_\gamma}|^2 |\sum_{\gamma'} C^{*\gamma'}_{ck'_2} C^{\gamma'}_{vk_2} e^{iQ\ell_\gamma}|^2 K_0(|Q|\delta)^2\right]$$
$$+ \left[\sum_{Q,k_2} |\sum_{\gamma} C^{\gamma *}_{ck'_1} C^{\gamma}_{vk_2} e^{-iQ\ell_\gamma}|^2 |\sum_{\gamma'} C^{\gamma' *}_{ck'_2} C^{\gamma'}_{ck_1} e^{-iQ\ell_{\gamma 2}}|^2 K_0(|Q|\delta)^2\right]$$
$$+ \left[\sum_{Q,k_2} Re|\sum_{\gamma} C^{\gamma *}_{ck'_1} C^{\gamma}_{ck_1} e^{-iQ\ell_\gamma} \sum_{\gamma'} C^{\gamma' *}_{ck'_2} C^{\gamma'}_{vk_2} e^{iQ\ell_{\gamma'}} \sum_{\gamma} C^{\gamma}_{ck'_1} C^{\gamma *}_{vk_2} \sum_{\gamma'} C^{\gamma'}_{ck'_2} C^{\gamma' *}_{ck_1} e^{-iQ\ell_{\gamma'}}\right]$$
$$\times K_0(|Q|\delta)^2 \delta(\varepsilon_{ck'_1} + \varepsilon_{ck_2} - \varepsilon_{ck_1} - \varepsilon_{ck'_2}) \tag{3.67}$$

CHAPTER 4

CONCLUSIONS

In conclusion, this thesis comprises a theoretical study on carrier dynamics in graphene and armchair nanoribbon. In the study of semiconductors, the carrier lifetimes is a key subject and play an important role in the design and performance of semiconductor devices. The non-radiative Auger process is a band-to-band recombination mechanism. Band-to-band recombination provides the ultimate limit to carrier lifetimes. In this thesis, we examine the inverse-Auger rate for bulk graphene and armchair nanoribbon by using the tight binding method. As an exceptional feature of the linear and gapless bandstructure, Auger processes is found to be a key factor in graphene.

Firstly, in this study, we study the electronic structure of the bulk graphene using tight binding method . Then, we calculate the inverse-Auger rate using the tight binding wave function for intravalley and intervalley scattering. We take into consideration only the electron-electron scattering mechanism for intravalley and intervalley processes. We develop a model for 2D systems. We obtain the generation rate at the order of $10^{17}s^{-1}$. According to our calculations, inverse-Auger effect in the bulk graphene provides the formation of new excitons which is approximately proportional to the energy of an electron at the conduction band. In chapter 3, we obtain the energy spectrum and wave function for armchair graphene nanoribbon by using the nearest-neighbor tight-binding model. Then we obtain the inverse Auger rate of the armchair graphene nanoribbon in terms of tight-binding parameters, and the width of the nanoribbon.

REFERENCES

[1] Randy J Ellingson, Matthew C Beard, Justin C Johnson, Pingrong Yu, Olga I Micic, Arthur J Nozik, Andrew Shabaev, and Alexander L Efros. Highly efficient multiple exciton generation in colloidal pbse and pbs quantum dots. *Nano letters*, 5(5):865–871, 2005.

[2] Peter T Landsberg. *Recombination in semiconductors*. Cambridge University Press, 2003.

[3] Franz Schulze, Mario Schoth, Ulrike Woggon, Andreas Knorr, and Carsten Weber. Ultrafast dynamics of carrier multiplication in quantum dots. *Physical Review B*, 84(12):125318, 2011.

[4] R. D. Schaller and V. I. Klimov. High efficiency carrier multiplication in pbse nanocrystals: Implications for solar energy conversion. *Phys. Rev. Lett.*, 92:186601, May 2004.

[5] Nathaniel M Gabor, Zhaohui Zhong, Ken Bosnick, Jiwoong Park, and Paul L McEuen. Extremely efficient multiple electron-hole pair generation in carbon nanotube photodiodes. *Science*, 325(5946):1367–1371, 2009.

[6] Justin B Sambur, Thomas Novet, and BA Parkinson. Multiple exciton collection in a sensitized photovoltaic system. *Science*, 330(6000):63–66, 2010.

[7] John A McGuire, Milan Sykora, Jin Joo, Jeffrey M Pietryga, and Victor I Klimov. Apparent versus true carrier multiplication yields in semiconductor nanocrystals. *Nano letters*, 10(6):2049–2057, 2010.

[8] Farhan Rana. Electron-hole generation and recombination rates for coulomb scattering in graphene. *arXiv preprint arXiv:0705.1204*, v2:13, 2007.

[9] S Winnerl, M Orlita, P Plochocka, P Kossacki, M Potemski, T Winzer, E Malic, A Knorr, M Sprinkle, C Berger, et al. Carrier relaxation in epitaxial graphene photoexcited near the dirac point. *Physical review letters*, 107(23):237401, 2011.

[10] Nathaniel M Gabor, Justin CW Song, Qiong Ma, Nityan L Nair, Thiti Taychatanapat, Kenji Watanabe, Takashi Taniguchi, Leonid S Levitov, and Pablo Jarillo-Herrero. Hot carrier–assisted intrinsic photoresponse in graphene. *Science*, 334(6056):648–652, 2011.

[11] KJ Tielrooij, JCW Song, SA Jensen, A Centeno, A Pesquera, A Zurutuza Elorza, M Bonn, LS Levitov, and FHL Koppens. Photoexcitation cascade and multiple hot-carrier generation in graphene. *Nature Physics*, 9(4):248–252, 2013.

[12] Torben Winzer, Andreas Knorr, and Ermin Malic. Carrier multiplication in graphene. *Nano letters*, 10(12):4839–4843, 2010.

[13] P Plochocka, P Kossacki, A Golnik, T Kazimierczuk, C Berger, WA de Heer, and M Potemski. Slowing hot-carrier relaxation in graphene using a magnetic field. *Physical Review B*, 80(24):245415, 2009.

[14] Satoru Konabe, Nobuhito Onoda, and Kazuyuki Watanabe. Auger ionization in armchair-edge graphene nanoribbons. *Physical Review B*, 82(7):073402, 2010.

[15] James McClain and Joshua Schrier. Multiple exciton generation in graphene nanostructures. *The Journal of Physical Chemistry C*, 114(34):14332–14338, 2010.

[16] Mark Wilson. Electrons in atomically thin carbon sheets behave like massless particles. *Physics Today*, 59(1):21–23, 2006.

[17] Yuanbo Zhang, Yan-Wen Tan, Horst L Stormer, and Philip Kim. Experimental observation of the quantum hall effect and berry's phase in graphene. *Nature*, 438(7065):201–204, 2005.

[18] Claire Berger, Zhimin Song, Xuebin Li, Xiaosong Wu, Nate Brown, Cécile Naud, Didier Mayou, Tianbo Li, Joanna Hass, Alexei N Marchenkov, et al. Electronic confinement and coherence in patterned epitaxial graphene. *Science*, 312(5777):1191–1196, 2006.

[19] Akin Akturk and Neil Goldsman. Electron transport and full-band electron-phonon interactions in graphene. *Journal of Applied Physics*, 103(5):053702, 2008.

[20] Philip Richard Wallace. The band theory of graphite. *Physical Review*, 71(9):622, 1947.

[21] Xue-Feng Wang and Tapash Chakraborty. Collective excitations of dirac electrons in a graphene layer with spin-orbit interactions. *Physical Review B*, 75(3):033408, 2007.

[22] Gordon W Semenoff. Condensed-matter simulation of a three-dimensional anomaly. *Physical Review Letters*, 53(26):2449–2452, 1984.

[23] Riichiro Saito, Gene Dresselhaus, Mildred S Dresselhaus, et al. *Physical properties of carbon nanotubes*, volume 4. World Scientific, 1998.

[24] Hartmut Haug and Stephan W Koch. *Quantum theory of the optical and electronic properties of semiconductors*, volume 3. World Scientific, 2004.

[25] Antónia Mošková and Martin Moško. Exchange carrier-carrier scattering of photoexcited spin-polarized carriers in gaas quantum wells: Monte carlo study. *Physical Review B*, 49(11):7443, 1994.

[26] TO Wehling, E Şaşıoğlu, C Friedrich, AI Lichtenstein, MI Katsnelson, and S Blügel. Strength of effective coulomb interactions in graphene and graphite. *Physical review letters*, 106(23):236805, 2011.

[27] Andrea Tomadin, Daniele Brida, Giulio Cerullo, Andrea C Ferrari, and Marco Polini. Nonequilibrium dynamics of photoexcited electrons in graphene: Collinear scattering, auger processes, and the impact of screening. *Physical Review B*, 88(3):035430, 2013.

[28] D Brida, A Tomadin, C Manzoni, YJ Kim, A Lombardo, S Milana, RR Nair, KS Novoselov, AC Ferrari, G Cerullo, et al. Ultrafast collinear scattering and carrier multiplication in graphene. *Nature communications*, 4, 2013.

[29] Luca Pirro, Anuj Girdhar, Yusuf Leblebici, and Jean-Pierre Leburton. Impact ionization and carrier multiplication in graphene. *Journal of Applied Physics*, 112(9):093707, 2012.

[30] Katsunori Wakabayashi, Ken-ichi Sasaki, Takeshi Nakanishi, and Toshiaki Enoki. Electronic states of graphene nanoribbons and analytical solutions. *Science and Technology of Advanced Materials*, 11(5):054504, 2010.

[31] Ken-ichi Sasaki, Katsunori Wakabayashi, and Toshiaki Enoki. Electron wave function in armchair graphene nanoribbons. *Journal of the Physical Society of Japan*, 80(4), 2011.

[32] Farhan Rana, Paul A George, Jared H Strait, Jahan Dawlaty, Shriram Shivaraman, Mvs Chandrashekhar, and Michael G Spencer. Carrier recombination and generation rates for intravalley and intervalley phonon scattering in graphene. *Physical Review B*, 79(11):115447, 2009.

APPENDIX A

TIGHT BINDING MODEL OF ZIGZAG NANORIBBON

A.1. Electronic Structure of Zigzag Nanoribbons

In this section, we obtain the energy spectrum and wave function of the zigzag ribbon by using the analytical solution of the nearest-neighbor tight-binding model [30]. The tight-binding Hamiltonian for zigzag nanoribbons can be explicitly written as

$$H = -t\sum_{\ell}\sum_{m=odd}^{N}[a_{\ell}^{\dagger}(m)b_{\ell-1}(m) + b_{\ell}^{\dagger}(m)a_{\ell}(m) + a_{\ell}^{\dagger}(m+1)b_{\ell}(m)] + h.c.$$
$$- t\sum_{\ell}\sum_{m=even}^{N} b_{\ell}^{\dagger}(m)a_{\ell-1}(m) + h.c. \tag{A.1}$$

The anticommutation relations is defined as

$$\{a_{\ell}(m), a_{\ell'}^{\dagger}(m')\} = \delta_{\ell,\ell'}\delta_{m,m'} \tag{A.2}$$

$$\{b_{\ell}(m), b_{\ell'}^{\dagger}(m')\} = \delta_{\ell,\ell'}\delta_{m,m'} \tag{A.3}$$

and other anticommutations are zero. The one-particle state is defined as

$$|\Psi(k)\rangle = \sum_{m}(\psi_{m,A}\alpha_{k}^{\dagger}(m) + \psi_{m,B}\beta_{k}^{\dagger}(m))|0\rangle \tag{A.4}$$

Inserting this one-particle state into the Schrödinger equation

$$H|\Psi(k)\rangle = E|\Psi(k)\rangle \tag{A.5}$$

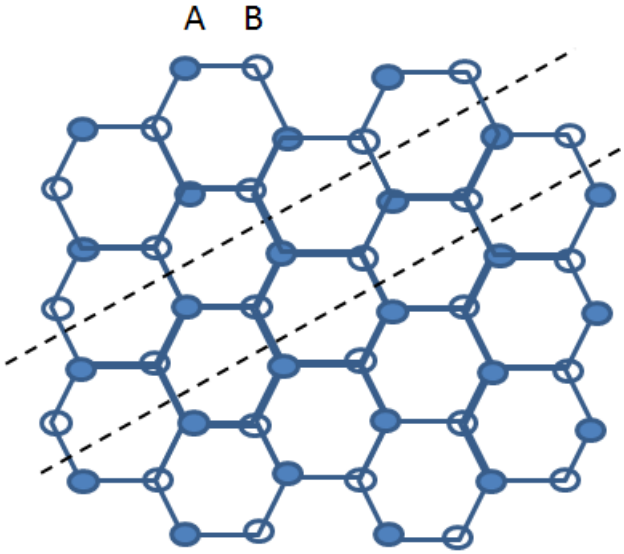

Figure A.1. The unit cell of zigzag nanoribbon.

we obtain the following set of equations of motion:

$$E\psi_{m,A} = -\psi_{m-1,B} - \rho\psi_{m,B} \tag{A.6}$$

$$E\psi_{m,B} = -\psi_{m+1,A} - \rho\psi_{m,A} \tag{A.7}$$

$$\rho = 2cos(\frac{k}{2}), m = 0, 1, 2, ..., N + 1 \tag{A.8}$$

The matrix elements of $N \times N$ submatrix $h_{AB}(k)$ can be written as for zigzag nanoribbons

$$h_{AB}(k) = \begin{pmatrix} 1+e^{ik} & 0 & 0 & \dots & \dots & 0 \\ 1 & 1+e^{ik} & 0 & 0 & \dots & 0 \\ 0 & 1 & 1+e^{ik} & 0 & \dots & 0 \\ \vdots & & \ddots & \ddots & \ddots & \vdots \\ \vdots & & 0 & 1 & 1+e^{ik} & 0 \\ 0 & \dots & \dots & 0 & 1 & 1+e^{ik} \end{pmatrix} \tag{A.9}$$

Because the 0B and (N + 1)A sites are missing, the equations of motion are modified at

the zigzag edge site to

$$E\psi_{1,A} = -\rho\psi_{1,B} \tag{A.10}$$

$$E\psi_{N,A} = -\rho\psi_{N,B} \tag{A.11}$$

Thus, the boundary condition for zigzag nanoribbons as

$$\psi_{0,B} = \psi_{N+1,A} = 0 \tag{A.12}$$

We assume

$$\psi_{m,A} = Ae^{ipm} + Be^{-ipm} \tag{A.13}$$

$$\psi_{m,B} = Ce^{ipm} + De^{-ipm} \tag{A.14}$$

Here A, B, C and D are arbitrary coefficients, which will be determined under the above boundary condition; p is the wavenumber in the transverse direction, which is also given by the boundary condition. From the boundary condition, we get the following relations

$$\psi_{0,B} = C + D \tag{A.15}$$

$$\psi_{N+1,A} = Az + Bz^{-1} = 0 \tag{A.16}$$

where z is defined as

$$z = e^{ip(N+1)} \tag{A.17}$$

$$\psi_{m,A} = A(e^{ipm} - z^2e^{-ipm}) \tag{A.18}$$

$$\psi_{m,B} = C(e^{ipm} - e^{-ipm}) \tag{A.19}$$

$$M\begin{pmatrix} A \\ B \end{pmatrix} = 0 \tag{A.20}$$

$$M = \begin{pmatrix} E(e^{ipm-z^2e^{-ipm}}) & (\rho + e^{-ip})e^{ipm} - (\rho + e^{-ip})e^{ipm} \\ (\rho + e^{ip})e^{ipm} - (\rho + e^{-ip})e^{-ipm}z^2 & E(e^{ipm} - e^{-ipm} \end{pmatrix} \tag{A.21}$$

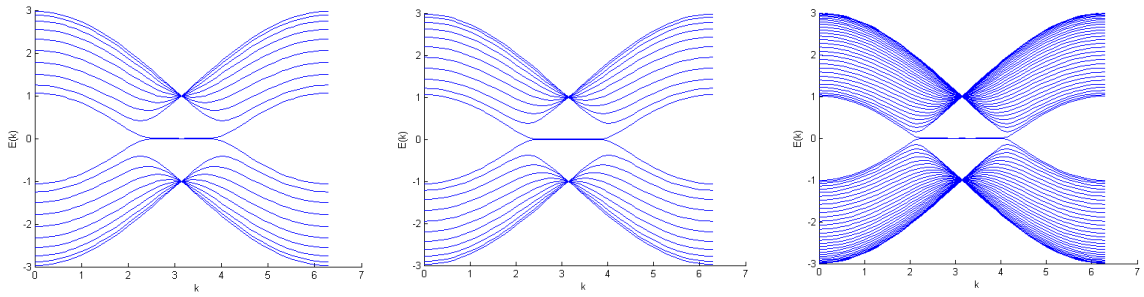

Figure A.2. The energy band structures of zigzag nanoribbons for N=10, N=11, N=30 respectively.

Matrix M is zero for the solutions of p for $-\pi, 0, \pi$.Therefore, we can find solutions that satisfy

$$detM = 0 \tag{A.22}$$

except when p for $-\pi, 0, \pi$. we can show that $detM = 0$ has the following form:

$$fe^{i2pm} + ge^{-i2pm} + x = 0 \tag{A.23}$$

where f, g and x are functions of E, ρ and z.

$$E^2 = (\rho + e^{ip}) + (\rho + e^{-ip}) = 1 + \rho^2 + 2\rho cos(p) \tag{A.24}$$

$$E_{\pm} = \pm\sqrt{1 + \rho^2 + 2\rho cos(p)} \tag{A.25}$$

The transverse wavenumber $p = p(k, N)$ is given as thr solution of the equation

$$sin[pN] + \rho sin[p(n+1)] = 0 \tag{A.26}$$

the wavefunction can be written as

$$\begin{pmatrix} \psi_{m,A} \\ \psi_{m,B} \end{pmatrix} = M \begin{pmatrix} \mp sin(p(N+1-m)) \\ sin(pm) \end{pmatrix} \tag{A.27}$$

with the normalization constant M.